Multiband optical variability of a newly discovered 12 blazars sample from 2013 – 2019

Miljana D. Jovanović [1,2]★ Goran Damljanović,[1] François Taris,[3] Alok C. Gupta[4,5] and Gopal Bhatta[6]

[1]*Astronomical observatory, Volgina 7, 11060 Belgrade, Serbia*

[2]*Department of Astronomy, Faculty of Mathematics, University of Belgrade, Studentski trg 16, 11000 Belgrade, Serbia*

[3]*Observatoire de Paris - SYRTE, 61 avenue de l'Observatoire 75014 Paris, France*

[4]*Key Laboratory for Research in Galaxies and Cosmology, Shanghai Astronomical Observatory, Chinese Academy of Sciences, Shanghai 200030, China*

[5]*Aryabhatta Research Institute of Observational Sciences (ARIES), Manora Peak, Nainital 263001, India*

[6]*Institute of Nuclear Physics PAN, Polish Academy of Sciences, PL–31342 Krakow, Poland*

ABSTRACT

Here we present the first optical photometric monitoring results of a sample of 12 newly discovered blazars from the ICRF – *Gaia* CRF astrometric link. The observations were performed from April 2013 to August 2019 using eight telescopes located in Europe. For a robust test for the brightness and colour variability, we use Abbé criterion and F-test. Moreover, linear fittings are performed to investigate the relation in the colour-magnitude variations of the blazars. Variability was confirmed in the case of 10 sources; two sources, 1429+249 and 1556+335 seem to be possibly variable. Three sources (1034+574, 1722+119, and 1741+597) have displayed large amplitude brightness change of more than one magnitude. We found that the seven sources displayed bluer-when-brighter variations, and one source showed redder-when-brighter variations. We briefly explain the various AGN emission models which can explain our results.

Key words: Galaxies: active – BL Lacertae objects: general – Quasars: general – Galaxies: photometry.

1 INTRODUCTION

Blazars form a subclass of radio loud (RL) active galactic nuclei (AGN) which eject relativistic jets along the observer's line of sight (Urry & Padovani 1995). BL Lacertae objects (BL Lacs) and flat spectrum radio quasars (FSRQs) are collectively referred to as blazars. In the composite optical/UV spectra, BL Lacs show featureless continuum or weak narrow emission lines (equivalent width EW ≤ 5 Å) (e.g. Stickel et al. 1991; Marcha et al. 1996) while FSRQs show prominent broad emission lines. Blazars flux, polarization, and spectra are highly variable in the whole (radio to γ-rays) electromagnetic (EM) spectrum (e.g. Gupta et al. 2017b, and references therein). Blazars in general show variability on diverse time-scales, ranging as short as a few minutes to as long as several decades. Variability time-scales of blazars can be broadly divided into three classes: time-scale from a few minutes to a less than a day is commonly known as microvariability (Miller, Carini & Goodrich 1989) or intra-day variability (IDV) (Wagner & Witzel 1995) or intra-night variability (Gopal-Krishna, Sagar & Wiita 1993). Variability time-scales ranging from a few days to a few months are called short-term variability (STV), and those from a few months to several years are termed as long-term variability (LTV; see Gupta et al. 2004).

Blazar emission extending across the entire EM spectrum is dominated by non-thermal radiation from the relativistic jets. The broad-band emission provides us an excellent opportunity to study their spectral energy distribution (SED), often characterized by well-known double-hump structure (von Montigny et al. 1995; Fossati et al. 1998). In all classes of blazars, from radio to soft X-ray frequencies the dominant emission mechanism is synchrotron emission, and whereas in hard X-ray and γ-ray energies it is most probably inverse Compton (IC) scattering (Ulrich, Maraschi & Urry 1997; Böttcher 2007). In the recent classification scheme based on the peak synchrotron frequency ν_{peak}, blazars are classified in three sub-classes: LSP – Low synchrotron peak with $\nu_{peak} \leq 10^{14}$ Hz, ISP – Intermediate synchrotron peak with $10^{14} < \nu_{peak} < 10^{15}$ Hz, and HSP – High synchrotron peak with $\nu_{peak} \geq 10^{15}$ Hz (Abdo et al. 2010).

The optical band is quite narrow in comparison to the other spectral bands over the entire EM spectrum. Nevertheless it helps us obtain important information regarding non-thermal synchrotron emission, as well as possible thermal emission from accretion disc. In general on STV and LTV time-scales, spectral trends of bluer-when-brighter (BWB) in BL Lacs and redder-when-brighter (RWB) in FSRQs have been observed, although occasionally opposite trends are also detected in some blazars (e.g. Gu et al. 2006; Gaur et al. 2012b; Isler et al. 2017, and references therein). In recent times, extensive studies on blazar optical variability on diverse time-scales have been carried out using observations from both space and ground based telescopes. The results demonstrate that the general nature of the LTV is mostly characterized by substantial change in the flux, which are occasionally accompanied by sudden flares and quasi-periodic oscillations (Bhatta et al. 2023). The blazars light curves often show normal or log-normal flux distribution (see Bhatta 2021). In shorter time-scales similar variability properties with power-law spectral

★ E-mail: miljana@aob.rs

Table 1. Optical observation log for the sample blazars.

IERS name	$\alpha_{J2000.0}(°)$	$\delta_{J2000.0}(°)$	z	AGN Type	Observation duration Date	Date	Number of observations V, R
0049+003	13.02321	0.593930	0.399714	FSRQ	2013 Sept 06	2019 Aug 08	30, 40
0907+336	137.65431	33.49012	0.354000	BL Lac	2013 Apr 14	2019 Apr 06	39, 42
1034+574	159.43461	57.19878	1.095700	BL Lac	2013 July 09	2019 Apr 07	47, 47
1212+467	183.79143	46.45420	0.720154	FSRQ	2013 July 09	2019 Mar 31	50, 50
1242+574	191.29167	57.16510	0.998229	BL Lac	2014 Apr 02	2019 Aug 06	49, 57
1429+249	217.85787	24.70575	0.406590	BL Lac/FSRQ	2014 Apr 02	2019 Aug 06	40, 44
1535+231	234.31043	23.01127	0.462515	BL Lac/FSRQ	2014 Apr 04	2019 Aug 06	43, 44
1556+335	239.72993	33.38850	1.653598	FSRQ	2014 Apr 04	2019 Aug 06	41, 50
1607+604	242.08560	60.30784	0.178000	BL Lac	2013 July 08	2019 Aug 06	42, 48
1612+378	243.69564	37.76869	1.531239	FSRQ	2013 July 09	2019 Aug 06	37, 42
1722+119	261.26810	11.87096	0.340000	BL Lac	2013 July 09	2019 Aug 08	43, 47
1741+597	265.63334	59.75186	0.415000	BL Lac	2013 July 09	2019 Aug 07	55, 62

density were reported in a large number of *TESS* blazar light curves (Pininti et al. 2023).

On 2022 June 13, the third data release (DR3) of *Gaia* mission was made available for public (*Gaia* Collaboration et al. 2022). The *Gaia* uses astrometric observations of optical counterparts of sources from the radio catalogue International Celestial Reference Frame (ICRF) (Charlot et al. 2020) to adjust its reference frame. A set of ~ 1.6 million quasi-stellar objects (QSOs) constitutes the third version of the *Gaia* celestial reference frame (*Gaia*-CRF3). 398 sources not included in the ICRF list were mentioned as potential sources for Very Long Baseline Interferometry (VLBI) observations (Bourda et al. 2010). From this list, 105 sources were observed with a global VLBI array which detected 47 point-like sources on VLBI scales and classified as AGNs (Bourda et al. 2011).

From 2013 to 2019, we conducted optical photometric observations in the *V* and *R* bands for 12 blazars selected from a sample of 47 AGNs detected in Bourda et al. (2011). Of the 12 blazars studied, 6 are classified as BL Lacs, 4 as FSRQs, and 2 exhibit characteristics of both BL Lacs and FSRQs. The detailed information about these blazars: their International Earth Rotation Service (IERS) name and observations log are provided in Table 1. In this work, we conduct a thorough investigation of the optical flux and colour variability properties of these blazars on both short-term and long-term time-scales.

The paper is structured as follows. In Section 2, we describe our new photometric observations. The detailed description of various analysis techniques used is explained in Section 3. Section 4 gives the results of individual AGN. Discussion and Conclusions are given in Section 5.

2 OBSERVATIONS AND PHOTOMETRY

The optical photometric observations of the blazars were performed using eight telescopes located in Europe. Out of these eight telescopes, two are stationed at Astronomical Station Vidojevica (ASV) of Astronomical Observatory of Belgrade, Serbia; one robotic Joan Oró telescope (TJO) at the Montsec Astronomical Observatory, Catalonia, Spain; four telescopes in Bulgaria of which three at Rozhen, NAO and one in Belogradchik; and one telescope at Leopold Figl observatory at Vienna, Austria. The details about these telescopes, their mirror aperture, mounted CCD cameras and optical filters are presented in Table 2.

During each observing night, two or more CCD image frames of the blazars were acquired in both the *V* and *R* bands. The image processing was performed using IRAF[1] scripting language (ascl: 9911.002) (Tody 1986, 1993). Bias, dark, and flat-field frames were obtained for every observing night, which were used for advanced image calibration and bad pixel mapping (dark frames for hot, and flat-field for dead pixel map). In addition, the corrections for cosmic rays were performed using Laplacian Cosmic Ray Identification method (van Dokkum 2001).

We performed differential photometry using Maxim DL software for determining the brightness of the sources with the aperture radius of ~6 arcsec. The details about differential photometry and selection of comparison and control stars are presented in papers Taris et al. (2018), and Jovanović (2019). The PSF *ugriz* (point spread function *u*, *g*, *r*, *i*, and *z*) magnitudes for the comparison and control stars were taken from the Sloan Digital Sky Survey Data Release 14 (SDSS DR14) catalogue (Abolfathi et al. 2018). The magnitudes in *V* and *R* bands were calculated from *g*, *r*, and *i* band magnitudes using the equations given by Chonis & Gaskell (2008). Except for source 1722+119 magnitudes *V* and *R* are taken from paper Doroshenko et al. (2014). The light curves of 1741+597 in V and R bands are presented in Fig. 1, for all sources the ligth curves are presented in Apendix A, and in Table 3.

3 ANALYSIS METHODS

To test for the presence of variability in the source, we performed two statistics: Abbé's criterion and F-test. Both of the tests require normal distribution of data (in some cases the Abbé' criterion can be applied when data distribution is different from normal (Lemeshko 2006)). We consider a light curve of the source as variable if the variability is detected by both test statistics. Before applying these statistical tests, we used 3σ rule (Pukelsheim 1994) and Shapiro–Wilk test of normality (Razali, Wah et al. 2011). We discarded some of the data which were obtained under poor weather conditions. We concluded that the statistical methods which require normal distribution of data can be applied.

---

[1]Image Reduction and Analysis Facility, a general purpose software system for the reduction and analysis of astronomical data. IRAF is distributed by the National Optical Astronomy Observatories, which are operated by the Association of Universities for Research in Astronomy, Inc., under cooperative agreement with the National Science Foundation.

Table 2. Details of telescopes and instruments.

| Telescope	ASV 60 cm	ASV 1.4 m	TJO 80 cm	Rozhen 2 m
CCD model	Apogee Alta E47	Andor iKon-L	Andor iKon-L	Andor iKon-L
	Apogee Alta U42	Apogee Alta U42	FLI PL4240-1-B	VersArray:1300B
	SBIG ST10 XME			
Chip size (pixels)	1024×1024	2048×2048	2048×2048	2048×2048
	2048×2048	2048×2048	2048×2048	1340×1300
	2184×1472			
Scale (arcsec pixel^{-1})	0.45	0.244	0.361	0.176
	0.466	0.244	0.364	0.258
	0.23			
Field (arcmin^2)	7.6×7.6	8.3×8.3	12.3×12.3	6.0×6.0
	15.8×15.8	8.3×8.3	12.3×12.3	5.76×5.76
	8.4×7.5			
Gain (e$^-$/ADU)	2.56	1	1	1.7
	1.25	1.25	1.5	1
	1.2			
Read-out Noise (e$^-$ rms)	37.2	7	13.7	6
	12.5	12.5	6.6	2
	8.8			
Typical seeing (arcsec)	$1-2$	$1-2$	$1-2$	$1.5-2.5$
Telescope	LFOA 1.5 m	Rozhen 50/70 cm	Rozhen 60 cm	Belogradchik 60 cm
CCD model	SBIG ST10 XME	FLI PL16803	FLI PL9000	FLI PL9000
Chip size (pixels)	2184×1472	4096×4096	3056×3056	3056×3056
Scale (arcsec/pixel)	0.15	1.079	0.33	0.33
Field (arcmin^2)	5.6×3.8	73.66×73.66	16.8×16.8	16.8×16.8
Gain (e$^-$/ADU)	1.42	1	1	1
Read-out noise (e$^-$ rms)	13.38	9	9	9
Typical seeing (arcsec)	$2-4$	$2-4$	$1.5-2.5$	$1.5-2.5$
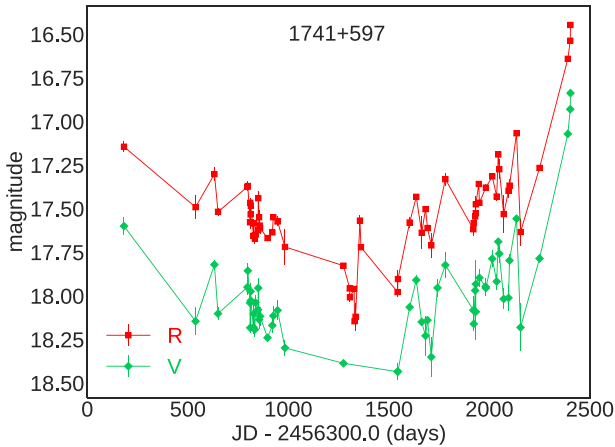
Figure 1. *V* (green diamonds) and *R* (red squares) band light curves of 1741+597 from 2013 July to 2019 August.

Table 3. Examples of observations from 2013 to 2019 in *V* and *R* bands.

Name	Julian date (JD)	Magnitude	Error	band
0049+003	2456542.47938	16.296	0.021	*V*
0049+003	2456542.49410	15.877	0.014	*R*
0049+003	2457011.29274	15.849	0.009	*R*
0049+003	2457011.29414	16.179	0.012	*V*
0049+003	2457011.34780	15.947	0.056	*R*
0049+003	2457011.34970	16.303	0.005	*V*

Note. This photometric data table is available in its entirety in a machine-readable form in the online journal. A portion is shown here for guidance regarding its form and content.

3.1 Abbé's criterion

We used Abbé's criterion to determine whether the elements of this sample are stochastically independent or not. Abbé's criterion is intended for checking hypotheses that all the observed quantities in the sample have identical mathematical expectations. The criterion is often used for checking the absence of systematic changes in a series of measurements. Abbé's statistic q is defined as the ratio of the Allan variance σ_{AV} and unbiased sample variance σ_D

$$q = \frac{\sigma_{AV}}{\sigma_D} = \frac{\frac{1}{2(n-1)}\sum_{i=1}^{n-1}(x_{i+1}-x_i)^2}{\frac{1}{n-1}\sum_{i=1}^{n}(x_i-\bar{x})^2} = \frac{1}{2}\frac{\sum_{i=1}^{n-1}(x_{i+1}-x_i)^2}{\sum_{i=1}^{n}(x_i-\bar{x})^2},\quad (1)$$

where $\bar{x}$ is the mean value of the magnitudes. If the sample size $n \geq 20$, q is distributed approximately normally with a mean at 1.0, and with a variance of $\frac{n-2}{(n-1)(n+1)}$ (Hald 1952; Strunov 2006). The Allan variance alone was used for testing variability of extra-galactic sources (e.g. Feissel-Vernier 2003; Gattano, Lambert & Le Bail 2018; Taris et al. 2018). Abbé's criterion is for unevenly sampled data which in general are obtained by observations using ground based telescopes. This is a simple and effective method for analysing an unevenly sample of astronomical observations as described in Spano et al. (2011), Malkin (2013). In Abbé's test, the critical point is defined as $q_c = 1 + u_\alpha/\sqrt{n + 0.5(1+u_\alpha)^2}$, where u_α is quantile of normal distribution for the significance level α. The hypothesis about stochastic independence of the sample units is accepted under $q > q_c$, otherwise the elements of the sample cannot be accepted as random and independent. In our case the sample consists of differences of magnitudes of comparison stars (A and B) and target blazars. Abbé's statistics which correspond to that data are q_A, and q_B. If q_A, and q_B are lower than q_C, for the significance level $\alpha = 0.001$, we conclude

Table 4. Statistical results of objects variability.

Name	Band	n	Abbé's criterion q_A, q_B, q_c	F-test F_1, F_2, F_3, F_c	M_{MAX} (mag)	M_{MIN} (mag)	$M_{AV} \pm \sigma_M$ (mag)	A (mag)	VAP per cent	Variable
0049+003	V	30	0.18, 0.15, 0.48	1.30, 20.64, 15.92, 3.29	16.731	16.166	16.461 ± 0.185	0.565	56.40	V
	R	40	0.15, 0.15, 0.54	1.23, 48.16, 39.14, 2.76	16.292	15.835	16.100 ± 0.147	0.457	45.61	V
0907+336	V	36	0.18, 0.19, 0.52	1.05, 11.54, 11.02, 2.93	16.704	15.899	16.226 ± 0.180	0.805	80.51	V
	R	39	0.13, 0.09, 0.54	1.05, 25.25, 24.10, 2.80	16.445	15.559	15.911 ± 0.191	0.886	88.56	V
1034+574	V	47	0.20, 0.21, 0.57	1.00, 83.77, 83.96, 2.54	16.919	15.545	16.086 ± 0.335	1.374	137.16	V
	R	47	0.23, 0.22, 0.57	1.01, 96.54, 97.13, 2.54	16.504	15.253	15.744 ± 0.328	1.251	124.82	V
1212+467	V	49	0.23, 0.23, 0.58	1.02, 51.11, 50.25, 2.49	18.150	17.282	17.645 ± 0.203	0.868	86.13	V
	R	49	0.19, 0.17, 0.58	1.06, 36.06, 33.89, 2.49	17.900	17.181	17.499 ± 0.186	0.719	71.54	V
1242+574	V	43	0.25, 0.26, 0.56	1.04, 28.77, 27.66, 2.66	18.167	17.371	17.710 ± 0.223	0.796	78.85	V
	R	51	0.24, 0.27, 0.59	1.10, 58.77, 64.44, 2.44	17.816	16.990	17.353 ± 0.229	0.826	82.01	V
1429+249	V	33	0.49, 0.51, 0.50	1.32, 3.49, 4.61, 3.09	17.614	17.134	17.417 ± 0.107	–	–	NV
	R	37	0.51, 0.50, 0.52	1.10, 2.56, 2.82, 2.89	17.343	17.076	17.197 ± 0.073	–	–	NV
1535+231	V	43	0.30, 0.31, 0.56	1.11, 31.34, 34.81, 2.66	19.036	18.133	18.472 ± 0.233	0.903	89.81	V
	R	44	0.15, 0.18, 0.56	1.12, 16.41, 18.34, 2.63	18.610	17.797	18.193 ± 0.214	0.813	80.68	V
1556+335	V	41	0.43, 0.57, 0.55	1.18, 2.80, 2.37, 2.73	17.581	17.350	17.459 ± 0.064	–	–	NV
	R	50	0.77, 0.63, 0.58	1.44, 1.23, 1.77, 2.46	17.080	16.886	16.988 ± 0.052	–	–	NV
1607+604	V	42	0.26, 0.27, 0.55	1.12, 23.81, 21.33, 2.69	17.677	17.152	17.400 ± 0.127	0.525	52.18	V
	R	48	0.38, 0.41, 0.58	1.23, 8.55, 6.97, 2.51	17.140	16.747	16.956 ± 0.095	0.393	39.02	V
1612+378	V	31	0.15, 0.15, 0.49	1.27, 12.90, 10.16, 3.22	17.128	16.686	16.895 ± 0.137	0.442	44.16	V
	R	36	0.11, 0.10, 0.52	1.02, 13.16, 12.93, 2.93	16.661	16.271	16.474 ± 0.111	0.390	38.94	V
1722+119	V	36	0.11, 0.12, 0.52	1.05, 202.59, 192.64, 2.93	16.780	14.888	15.571 ± 0.467	1.892	189.06	V
	R	40	0.11, 0.11, 0.54	1.00, 1389.46, 1387.88, 2.76	16.343	14.371	15.083 ± 0.477	1.972	197.16	V
1741+597	V	55	0.26, 0.27, 0.60	1.05, 40.03, 41.84, 2.36	18.435	16.837	17.975 ± 0.313	1.598	159.37	V
	R	62	0.21, 0.21, 0.62	1.03, 33.84, 34.79, 2.24	18.145	16.447	17.513 ± 0.310	1.698	169.71	V

Note. In the Variable column, V represents variable, and NV non-variable source.

that there are statistically significant systematic variations present in the data.

3.2 F-test

We used F-test to determine the existence of brightness variability in the sample of blazars by following the method descibed in (e.g. de Diego 2010; Gupta et al. 2017a; Jovanović 2019, and references therein). We investigated variances of two data sets X and Y to test if they are equal to each other. The tested hypothesis is H_0: $VarX = VarY$, and alternative H: $VarX > VarY$. The corresponding statistic is

$$F = \frac{VarX}{VarY}. \qquad (2)$$

To implement the F-test to our sample, we calculate statistics: F_A, F_B, and its ratio $F_{A/B}$. The indices of statistics correspond to the data sets which are tested. X refers to the differences of magnitudes of targets and comparison stars A or B, the statistics are F_A or F_B, respectively. Y refers to the differences of magnitudes of comparison stars. The three $F_{A, B, A/B}$ statistics are compared with the critical values. The $F_{A/B}$ value should be $\sim$1, because it is expected that the tested brightness should be variable in the same manner for both comparison stars (A and B). When the F_A and F_B values are greater than critical ones (which correspond to the significance level 0.001, and number of freedom $n - 1$, where n is the sample size), the null hypothesis (of non-variability) is discarded.

3.3 Amplitude of variability

The percentage of magnitude variations can be calculated by using the variability amplitude parameter (VAP), which was introduced by

Heidt & Wagner (1996) and defined as

$$VAP = 100\sqrt{(M_{MAX} - M_{MIN})^2 - 2\sigma^2}\,(\%), \qquad (3)$$

where M_{MAX} and M_{MIN} are the maximum, and minimum magnitude of the sources, and σ is the average measurement error.

The statistical results are listed in Table 4. The columns are: name of sources, band, number of data, results of Abbé criterion, results of F-test, maximum (M_{MAX}), minimum (M_{MIN}), average (M_{AV}) magnitudes, amplitudes of full observations ($A = M_{MAX} - M_{MIN}$), and VAP.

3.4 Colour variability

In addition to the brightness variations, we also estimated colour variations of the blazars with respect to total duration of observations, and also with respect to R magnitude. Studying colour variations is of importance to characterize the nature of the variations in the blazars which help explain the dominant emission mechanism. For all the blazars, we generate diagrams of colour $V - R$ with respect to R magnitude (colour–magnitude diagram (CMD)), and colour ($V - R$) with respect to time (Julian days). For linear regression, Pearson's correlation coefficient with null hypothesis probability were estimated on the data of these CMDs and colour verses time plots. The positive slope, of linear regression of the data in CMD, is an indication of BWB, and negative are indications of RWB trend. The colour versus time and colour versus magnitude diagrams are presented for the most variable source in Figs 2 and 3, and for the all sources in Appendices B and C. The coefficients of linear regression (slope and intercept) and Pearson's correlation coefficients with probability are given in Tables 5 and 6, for colour-time and CMDs, respectively. If Pearson's coefficient r is positive and probability (of no correlation) P is lower than
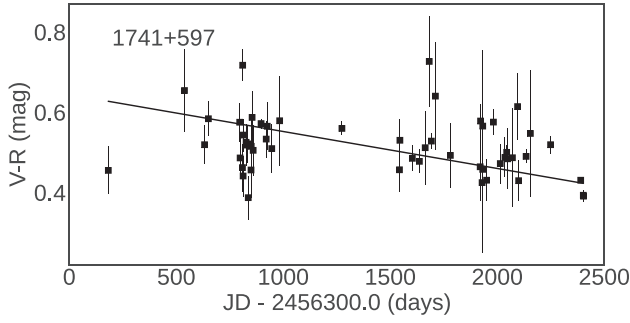
Figure 2. The light curve of colour indices $V - R$ variability during period 2013 July – 2019 August of 1741+597. Details about the colour variability of all sources can be found in Table 5.
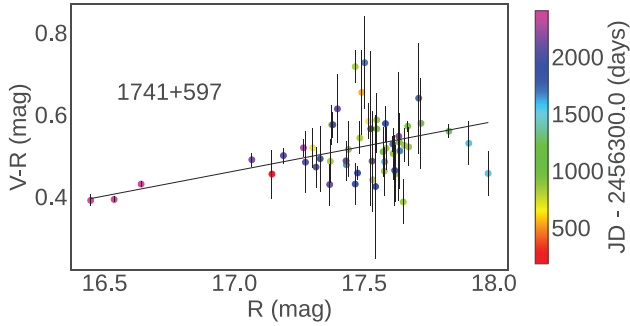

Figure 3. The correlation between colour indices $V - R$ and R-band magnitude of 1741+597. The colour bars indicate the progression of time. Details about the colour–magnitude correlations for all sources can be found in Table 6.

Table 5. The colour variations with respect to time.

Source	Slope ($\times 10^{-5}$)	Intercept	r	P
0049+003	4.0 ± 0.4	0.331 ± 0.007	0.52	3.10×10^{-3}
0907+336	− 4.7 ± 0.5	0.373 ± 0.005	− 0.53	6.00×10^{-4}
1034+574	1.0 ± 0.3	0.322 ± 0.004	0.16	2.82×10^{-1}
1212+467	− 2.3 ± 1.2	0.166 ± 0.012	− 0.15	2.97×10^{-1}
1242+574	− 0.3 ± 0.5	0.393 ± 0.010	− 0.03	8.20×10^{-1}
1429+249	0.5 ± 0.5	0.205 ± 0.009	0.06	7.19×10^{-1}
1535+231	− 2.1 ± 1.5	0.277 ± 0.027	− 0.12	4.54×10^{-1}
1556+335	0.4 ± 0.5	0.465 ± 0.009	0.06	7.34×10^{-1}
1607+604	4.1 ± 0.5	0.375 ± 0.007	0.58	1.00×10^{-4}
1612+378	1.3 ± 0.5	0.417 ± 0.006	0.23	1.72×10^{-1}
1722+119	0.1 ± 0.3	0.427 ± 0.005	0.02	8.77×10^{-1}
1741+597	− 9.2 ± 0.6	0.644 ± 0.012	− 0.79	1.46×10^{-12}

Notes. Slope, and Intercept of $V - R$ against JD-2456300 d,
r – Pearson's coefficient and P – null hypothesis probability.

0.05, we assume that the BWB colour-magnitude variation in source is present, if r is negative (and $P < 0.05$) we consider that RWB variation is present. In case of $P > 0.95$, we can conclude that the correlation is not present in colour-magnitude data. In other cases we can not conclude anything about behaviour of the process. In the similar manner as in Sections 3.1 and 3.2 we tested colour $V - R$ indices of objects control stars, and the results are presented in paper Jovanović, Damljanović & Taris (2023) – in Press.

Table 6. The colour – magnitude dependencies.

Source	Slope	Intercept	r	P
0049+003	0.189 ± 0.018	− 2.64 ± 0.29	0.56	1.40×10^{-3}
0907+336	− 0.093 ± 0.013	1.81 ± 0.20	− 0.39	1.38×10^{-2}
1034+574	0.033 ± 0.007	− 0.19 ± 0.11	0.27	6.67×10^{-2}
1212+467	− 0.055 ± 0.036	1.11 ± 0.63	− 0.12	4.07×10^{-1}
1242+574	− 0.013 ± 0.022	0.61 ± 0.38	− 0.04	8.11×10^{-1}
1429+249	0.226 ± 0.059	− 3.68 ± 1.02	0.24	1.34×10^{-2}
1535+231	− 0.082 ± 0.055	1.73 ± 1.01	− 0.13	4.11×10^{-1}
1556+335	− 0.096 ± 0.060	2.11 ± 1.01	− 0.12	4.64×10^{-1}
1607+604	0.302 ± 0.038	− 4.69 ± 0.64	0.56	1.00×10^{-4}
1612+378	0.175 ± 0.022	− 2.44 ± 0.36	0.61	1.00×10^{-4}
1722+119	0.024 ± 0.005	0.08 ± 0.07	0.37	1.41×10^{-2}
1741+597	0.121 ± 0.007	− 1.60 ± 0.12	0.86	1.43×10^{-16}

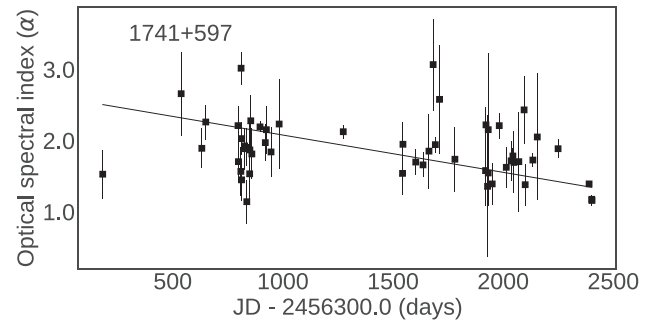*Note.* Slope and Intercept of $V - R$ against R, r – Pearson's coefficient, and P – null hypothesis probability.

Figure 4. The light curve of optical spectral indices variability during period 2013 July – 2019 August of 1741+597. Details about the α variability of all sources can be found in Table 7.

3.5 Spectral variability

The flux density can be described by power-law $F_\nu \propto \nu^\alpha$, where ν is frequency, and α is the spectral index. For the optical V and R bands, we calculated spectral index (similar to that presented for radio frequencies in paper Zajaček et al. 2019):

$$\alpha = \frac{\log(F_V/F_R)}{\log(\nu_V/\nu_R)}, \tag{4}$$

where F_V and F_R are fluxes of effective frequencies of V and R bands (ν_V and ν_R), respectively. With flux magnitude relation equation (4) can be written as

$$\alpha = \frac{c - 0.4(V - R)}{\log(\nu_V/\nu_R)}, \tag{5}$$

where $c = \log(ZP_V/ZP_R)$, ZP_V, and ZP_R are fluxes for magnitudes $V = 0$ and $R = 0$, respectively. The values ν_V, ν_R, ZP_V, and ZP_R were taken from Bessell, Castelli & Plez (1998).

The uncertainty of the spectral index σ_α was calculated as in Zajaček et al. (2019).

$$\sigma_\alpha = \frac{1}{|\log(\nu_V/\nu_R)|}\sqrt{(\sigma_{F_V}/F_V)^2 + (\sigma_{F_R}/F_R)^2}, \tag{6}$$

σ_{F_V} and σ_{F_R} are the uncertainties of flux densities at frequencies in V and R bands.

Our sample consists of three FSRQs, one ISP, and four HSPs sources. Spectral indices α in the optical band against synchrotron peak frequency ($\log \nu$) are presented in Fig. 6, with triangles are marked FSRQs, circle ISP, and squares HSPs. Synchrotron peak
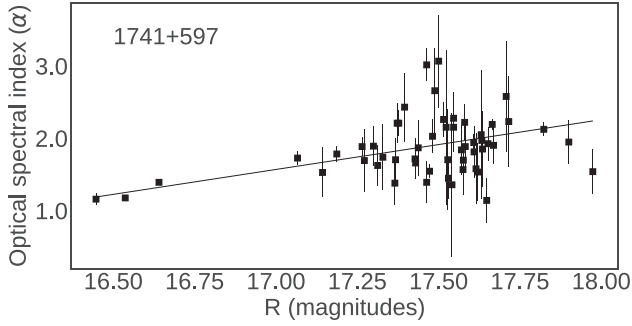
Figure 5. The correlation between optical spectral indices and *R*-band magnitude of 1741+597. Details about the α–*R* magnitude correlations for all sources can be found in Table 8.
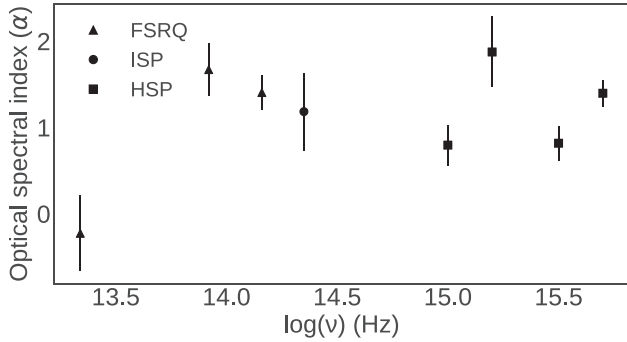

Figure 6. Average optical spectral index versus synchrotron peak frequency. Sources 0049+003, 1429+249, 1535+231, and 1607+604 are excluded because their sub-class could not be determined.

frequencies of these sources were taken from Mao & Urry (2017) and Chang et al. (2017, 2019).

The optical spectral index versus time and versus magnitude diagrams are presented for the most variable source in Figs. 4 and 5, and for the remaining sources in Appendices E and F. The mean optical spectral index α is negative for FSRQ 1212+467 ($\alpha = -0.23 \pm 0.44$), lower than 1 for two HSPs 0907+336 ($\alpha = 0.80 \pm 0.24$), and 1034+574 ($\alpha = 0.82 \pm 0.20$), and greater than 1 for two FSRQs 1556+335 ($\alpha = 1.67 \pm 0.30$), and 1612+378 ($\alpha = 1.41 \pm 0.20$), ISP 1242+574 ($\alpha = 1.18 \pm 0.45$), and two HSPs 1722+119 ($\alpha = 1.40 \pm 0.15$), and 1741+597 ($\alpha = 1.87 \pm 0.41$). For four sources (0049+003, 1429+249, 1535+231, and 1607+604) for which the synchrotron peak frequency is not available, their subclass could not be determined, but the α is calculated and the average values are 1.22 ± 0.30, 0.16 ± 0.36, 0.35 ± 0.73, and 1.51 ± 0.40, respectively.

3.6 SED

For nights when observations were obtained in the *B*, *V*, and *R* bands, the calibrated magnitudes of 12 blazars were dereddened by subtracting Galactic extinction $A_{B,V,R}$ (see Table 9). The presented values of $A_{B,V,R}$ were calculated using the NASA Extragalactic Data base Extinction calculator tool[2] (for *B*, *V*, and *R* bands it is based on paper Schlafly & Finkbeiner 2011). The SEDs are compiled using extinction corrected flux densities (F_ν) at *B*, *V*,
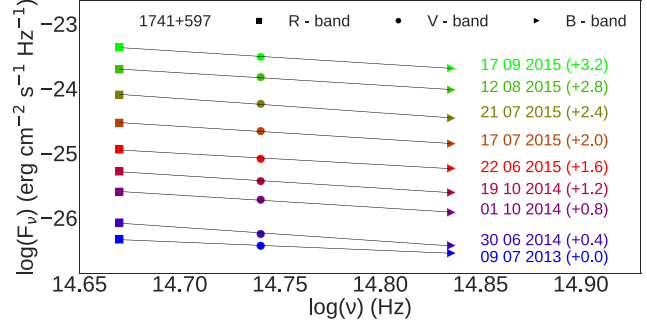
Figure 7. The SED of 1741+597 in *B*, *V*, and *R* bands. Details about the $\log F_\nu$–$\log \nu$ correlations for all sources can be found in Table 10.

Table 7. The spectral index variations with respect to time.

Source	Slope ($\times 10^{-5}$)	Intercept	r	P
0049+003	2.3 ± 2.0	0.83 ± 0.04	0.52	3.30×10^{-3}
0907+336	-2.7 ± 3.0	1.06 ± 0.03	-0.53	6.00×10^{-4}
1034+574	5.0 ± 2.0	0.78 ± 0.03	0.15	3.06×10^{-1}
1212+467	-1.3 ± 7.0	-0.11 ± 0.07	-0.15	2.95×10^{-1}
1242+574	-2.0 ± 3.0	1.17 ± 0.06	-0.03	8.31×10^{-1}
1429+249	3.0 ± 3.0	0.11 ± 0.05	0.06	7.19×10^{-1}
1535+231	-1.2 ± 9.0	0.52 ± 0.16	-0.12	4.54×10^{-1}
1556+335	3.0 ± 3.0	1.59 ± 0.05	0.06	7.15×10^{-1}
1607+604	2.3 ± 3.0	1.08 ± 0.04	0.58	1.00×10^{-4}
1612+378	7.0 ± 2.0	1.31 ± 0.03	0.23	1.72×10^{-1}
1722+119	1.0 ± 2.0	1.37 ± 0.03	0.03	8.70×10^{-1}
1741+597	-5.2 ± 3.0	2.60 ± 0.07	-0.79	1.54×10^{-12}

Notes. Slope, and Intercept of α against JD-2456300 d,
r – Pearson's coefficient, and P – null hypothesis probability.

and *R* wavelengths. Fig. 7 shows optical SED for 1741+597 for 9 different epochs. In Appendix D are presented optical SEDs for all sources, and the details (results of linear fits) are presented in Table 10.

4 RESULTS OF INDIVIDUAL TARGETS

Abbé's criterion and F-test show that the objects are variable in *V* and *R* bands in relation to both comparison stars A and B with exception of two objects. The $1424 + 249$ is considered to be variable in relation to a comparison star A according to Abbé's criterion in both bands, and in relation to B in according to Abbé's criterion in *R* band, and F-test in both bands. The object 1556+335 is variable only in *V* band in relation to star A. Magnitudes of sources 1212+467, 1242+574, 1535+231, and 1741+597 are not homogeneous in relation to the standard deviation. When the sources were fainter, the standard deviation was greater, and vice versa. Also, the colour of sources was tested using the same statistical tests, both tests did not show that the colour is variable. Optical variabilities of sources 0907+336, 1034+574, 1212+467, 1242+574, 1607+604, 1612+378, and 1722+119 in *B* and *R* bands were investigated by Abrahamyan et al. (2019). Their optical variability was classified as low.

The data from 2013 to 2015 were part of the data which were used for analysing variability of the sources, and the results were presented in paper Taris et al. (2018). For sources 1535+231, 1556+335, 1607+604, 1722+119, and 1741+597 data from 2016 to 2019 were used for testing comparison stars for differential photometry in

Table 8. The optical spectral index – magnitude dependencies.

Source	Slope	Intercept	r	P
0049+003	1.07 ± 0.10	-16.08 ± 1.64	0.56	1.40×10^{-3}
0907+336	-0.53 ± 0.07	9.21 ± 1.13	-0.39	1.38×10^{-2}
1034+574	0.19 ± 0.04	-2.13 ± 0.61	0.27	6.68×10^{-2}
1212+467	-0.32 ± 0.20	5.32 ± 3.57	-0.12	3.99×10^{-1}
1242+574	-0.07 ± 0.12	2.41 ± 2.17	-0.04	8.08×10^{-1}
1429+249	1.28 ± 0.34	-21.93 ± 5.79	0.24	1.34×10^{-1}
1535+231	-0.46 ± 0.31	8.78 ± 5.71	-0.13	4.11×10^{-3}
1556+335	-0.55 ± 0.34	10.97 ± 5.80	-0.12	4.64×10^{-1}
1607+604	1.71 ± 0.21	-27.67 ± 3.62	0.56	1.00×10^{-4}
1612+378	0.99 ± 0.13	-14.91 ± 2.07	0.61	1.00×10^{-4}
1722+119	0.13 ± 0.03	-0.59 ± 0.43	0.36	1.72×10^{-2}
1741+597	0.69 ± 0.04	-10.10 ± 0.68	0.86	1.67×10^{-16}

Notes. Slope, and Intercept of α against R, r – Pearson's coefficient, and P – null hypothesis probability.

Table 9. The Galactic extinction.

Source	A_B (mag)	A_V (mag)	A_R (mag)
0049+003	0.088	0.066	0.052
0907+336	0.079	0.060	0.047
1034+574	0.015	0.011	0.009
1212+467	0.052	0.040	0.031
1242+574	0.040	0.030	0.024
1429+249	0.119	0.090	0.071
1535+231	0.149	0.113	0.089
1556+335	0.111	0.084	0.067
1607+604	0.051	0.038	0.030
1612+378	0.057	0.043	0.034
1722+119	0.625	0.473	0.374
1741+597	0.157	0.119	0.094

Note. A_B, A_V, and A_R are galactic absorption for B, V, and R bands.

Jovanovic, Damljanovic & Vince (2018), and for obtaining their long-term period variability with Least Squares Method (LSM) iteratively in paper Jovanović (2019), analogously periodicity analysis for these blazars in short and long time-scales was performed in Jovanović & Damljanović (2020) as well as colour variability one in Jovanović et al. (2020). For the same sources the data from 2013 to 2019 were used for obtaining the periods of short and long term variations with LSM iteratively which was presented in paper Damljanović, Taris & Jovanović (2020). Moreover, the data (2013 – 2019) were used for testing the control stars for differential photometry (Jovanović, Damljanović & Taris (2021), and Jovanović et al. (2023) – in Press).

4.1 0049+003

The source was first detected by *HEAO-2* onboard of the *Einstein* satellite (Harris et al. 1996). The large bright quasar survey identified it as a quasar through its spectrum and the redshift was found to be $z = 0.399$ (Hewett, Foltz & Chaffee 1995). Later using another spectral analysis its redshift estimation was confirmed and found that $z = 0.399714$ (Richards et al. 2015). Healey et al. (2007) classified it as an FSRQ. The absolute magnitude of the source was estimated to be $M_I = -25.48$ (Meusinger, Hinze & de Hoon 2011). In paper Jun & Im (2013) source was catalogued as the hot dust-poor quasar with logarithm of the mass of the central black hole and the ratio of bolometric luminosity to Eddington luminosity $8.43 \pm 0.01 \, M_\odot$ and 0.959 ± 0.030, respectively, something similar was derived in paper Rakshit, Stalin & Kotilainen (2020) 8.425803 ± 0.018190, and logarithmic Eddington ratio -0.183588. In optical radio correlation

study with optical data from SDSS and radio data from FIRST surveys, the optical/radio morphology of the object was classified as the optical/radio emission from the core of the source and extended radio jet emission in papers de Vries et al. (2004), and Kimball et al. (2011). Comparing two epochs of FIRST survey with the higher angular resolution data of 1.4 GHz survey of SDSS Stripe 82, two diffuse lobes were visible on either side of the core and morphological class of source was defined as: core-lobe morphology (core is surrounded by two distinct non-variable lobe components Hodge et al. 2013). Gu & Ai (2011) investigate the optical variability in *r* band using SDSS DR7 which released multi-epoch data covering about nine years. The source shows variation of $\Delta r = 0.44$ mag.

During our monitoring, the brightness changed by ∼0.5 magnitudes in *V* and *R* bands. The colour of the blazar has changed by ∼0.2 magnitude during observational duration and shows BWB variations. The BWB variations can be seen in Fig. C1 (colour–magnitude diagram) in Appendix C.

4.2 0907+336

The source is also known as Ton 1015 and was for the first time noticed at the Tonantzintla Observatory in the second survey of blue stars in the north galactic pole, and its photographic magnitude was estimated to be 16 ± 0.5 (Chavira 1959). The source was detected in the radio band in a survey of faint sources at 5 GHz radio band by National Radio Astronomy Observatory (NRAO) (Davis 1971). In the cross-identification of optical and radio sources, the object was classified as a BL Lac and the redshift was estimated $z = 0.354$ from spectrum (Bauer et al. 2000). Its synchrotron peak frequency $\nu_{peak} = 10^{14.48}$ Hz was estimated and classified as an ISP, and radio to optical spectral index was found to be 0.28 in Fan et al. (2016). In other studies the source is classified as an HSP (e.g. Nieppola, Tornikoski & Valtaoja 2006; Ackermann et al. 2011; Chang et al. 2017; Mao & Urry 2017). We classify the source as HSP according to the value for $\nu_{peak} = 10^{15.0}$ from Chang et al. (2017). Using broad-band SED modelling with synchrotron self-Compton (SSC)/Thomson model, its jet parameters were estimated (Chen 2018).

We noticed that in both bands the brightness decreases by ∼0.8 magnitude. A few outbursts in both bands occurred, three between 2014 March 01 and 2016 May 16, and one between 2017 October 18 and 2018 October 04. The colour also decreased by ∼0.2 magnitude during our observations. From colour–magnitude dependencies, we conclude that RWB variation is present, the colour index is smaller when the brightness of the blazar decreases, see Fig. C1 and Table 6.

4.3 1034+574

The source was discovered during Green Bank 4.85 GHz survey with NRAO 91-m telescope. The telescope was used for three surveys in 1986, 1987, and 1988, and two catalogues which contain this object were published in Becker, White & Edwards (1991), and Gregory & Condon (1991). The first time source was classified as BL Lac in paper Nass et al. (1996). The spectroscopic redshift $z = 1.0957$, together with absolute *i* magnitude -28.8, and the mass of the central black hole $10^{9.89655} \, M_\odot$ were determined during the Large Sky Area Multi-Object Fibre Spectroscopic Telescope (LAMOST) Quasar Survey (Dong et al. 2018). The classification of the source by synchrotron peak frequency position was discussed in a few papers. In the beginning the source was classified as ISP (Nieppola et al. (2006) and Ackermann et al. (2011)), and later as HSP (Fan et al. 2016; Mao & Urry 2017; Chang et al. 2019). We adopted for

Table 10. Straight-line fits to optical SEDs of 12 sources.

Observation date	Slope	Intercept	r	P	Observation date	Slope	Intercept	r	P
				Source					
				0049+003					
2013 Sept 06	-1.081 ± 0.077	-9.99 ± 1.13	-0.998	0.045	2015 Aug 15	-1.530 ± 0.169	-3.49 ± 2.49	-0.994	0.070
2014 Dec 19	-1.260 ± 0.175	-7.38 ± 2.58	-0.990	0.088	2015 Sept 13	-1.665 ± 0.306	-1.50 ± 4.52	-0.983	0.116
				0907+336					
2013 Apr 14	-0.862 ± 0.003	-13.11 ± 0.05	-1.000	0.003	2014 May 22	-0.982 ± 0.061	-11.36 ± 0.90	-0.998	0.039
2014 Mar 01	-1.033 ± 0.016	-10.64 ± 0.23	-1.000	0.010	2014 Oct 21	-1.016 ± 0.101	-10.81 ± 1.49	-0.995	0.063
				1034+574					
2013 July 09	-1.129 ± 0.075	-9.56 ± 1.11	-0.998	0.043	2014 May 22	-1.162 ± 0.073	-8.82 ± 1.08	-0.998	0.040
2014 Mar 01	-1.255 ± 0.040	-7.58 ± 0.59	-0.999	0.020	2015 Feb 19	-1.282 ± 0.188	-6.81 ± 2.77	-0.989	0.093
				1212+467					
2013 July 09	-0.097 ± 0.133	-25.02 ± 1.96	-0.591	0.598	2014 Dec 24	0.082 ± 0.203	-27.75 ± 3.00	0.374	0.756
2014 Apr 01	-0.182 ± 0.106	-23.84 ± 1.57	-0.864	0.336	2015 Feb 21	-0.112 ± 0.121	-24.81 ± 1.79	-0.678	0.526
2014 June 27	-0.112 ± 0.161	-24.96 ± 2.38	-0.571	0.613					
				1242+574					
2014 Apr 02	-1.160 ± 0.055	-9.42 ± 0.82	-0.999	0.030	2014 July 04	-1.392 ± 0.157	-6.13 ± 2.31	-0.994	0.071
2014 May 22	-1.151 ± 0.131	-9.71 ± 1.94	-0.994	0.072	2014 Dec 25	-1.274 ± 0.033	-7.78 ± 0.48	-1.000	0.016
2014 June 28	-1.359 ± 0.087	-6.62 ± 1.29	-0.998	0.041	2015 May 14	-1.756 ± 0.221	-0.60 ± 3.27	-0.992	0.080
				1429+249					
2014 Apr 04	-2.657 ± 2.310	12.96 ± 34.08	-0.755	0.456	2014 Dec 25	-2.954 ± 2.139	17.37 ± 31.55	-0.810	0.399
2014 June 28	-2.853 ± 2.328	15.85 ± 34.33	-0.775	0.436	2015 Apr 15	-2.858 ± 2.243	15.91 ± 33.08	-0.787	0.424
2014 July 04	-2.789 ± 2.390	14.89 ± 35.24	-0.759	0.451	2015 July 16	-3.063 ± 2.259	18.93 ± 33.31	-0.805	0.405
				1535+231					
2014 Apr 04	-0.725 ± 0.118	-16.26 ± 1.75	-0.987	0.103	2014 Dec 25	-0.757 ± 0.047	-15.74 ± 0.70	-0.998	0.040
2014 May 25	-0.413 ± 0.172	-20.87 ± 2.54	-0.923	0.251	2015 July 12	-0.733 ± 0.109	-15.94 ± 1.61	-0.989	0.094
2014 June 27	-0.654 ± 0.277	-17.34 ± 4.08	-0.921	0.255	2015 July 18	-0.799 ± 0.235	-15.01 ± 3.47	-0.959	0.182
				1556+335					
2014 Apr 04	-1.441 ± 0.046	-5.10 ± 0.68	-0.999	0.020	2015 Apr 20	-1.483 ± 0.063	-4.51 ± 0.94	-0.999	0.027
2014 June 27	-1.354 ± 0.084	-6.38 ± 1.24	-0.998	0.039	2015 July 12	-1.613 ± 0.069	-2.61 ± 1.02	-0.999	0.027
2014 July 04	-1.514 ± 0.017	-4.05 ± 0.25	-1.000	0.007					
				1607+604					
2013 July 08	-1.025 ± 0.044	-11.24 ± 0.65	-0.999	0.028	2014 July 03	-0.967 ± 0.010	-12.04 ± 0.15	-1.000	0.007
2014 Mar 01	-0.729 ± 0.100	-15.57 ± 1.48	-0.991	0.087	2014 Oct 10	-1.203 ± 0.087	-8.62 ± 1.29	-0.997	0.046
2014 May 28	-0.753 ± 0.135	-15.19 ± 1.99	-0.984	0.113	2015 June 12	-1.659 ± 0.043	-1.96 ± 0.63	-1.000	0.016
2014 June 28	-0.697 ± 0.100	-16.01 ± 1.47	-0.990	0.090	2015 July 17	-1.936 ± 0.157	2.10 ± 2.31	-0.997	0.051
				1612+378					
2013 July 08	-0.890 ± 0.044	-12.98 ± 0.64	-0.999	0.031	2014 Oct 01	-0.995 ± 0.077	-11.44 ± 1.13	-0.997	0.049
2014 May 28	-0.786 ± 0.172	-14.50 ± 2.54	-0.977	0.137	2015 June 14	-1.093 ± 0.138	-10.04 ± 2.03	-0.992	0.080
2014 June 29	-0.858 ± 0.224	-13.44 ± 3.30	-0.968	0.162	2015 July 18	-1.119 ± 0.125	-9.66 ± 1.85	-0.994	0.071
				1722+119					
2013 July 09	-1.042 ± 0.020	-10.01 ± 0.29	-1.000	0.012	2015 July 13	-1.242 ± 0.225	-7.13 ± 3.32	-0.984	0.114
2014 June 29	-1.052 ± 0.026	-9.75 ± 0.39	-1.000	0.016	2015 Aug 11	-1.289 ± 0.146	-6.49 ± 2.15	-0.994	0.072
2015 Apr 22	-1.225 ± 0.153	-7.52 ± 2.26	-0.992	0.079	2015 Sept 17	-1.306 ± 0.120	-6.27 ± 1.77	-0.996	0.058
2015 May 13	-1.005 ± 0.136	-10.75 ± 2.00	-0.991	0.085					
				1741+597					
2013 July 09	-1.273 ± 0.053	-7.67 ± 0.78	-0.999	0.027	2015 July 17	-1.957 ± 0.060	2.18 ± 0.89	-1.000	0.020
2014 June 30	-2.129 ± 0.181	4.75 ± 2.68	-0.996	0.054	2015 July 21	-2.197 ± 0.087	5.74 ± 1.29	-0.999	0.025
2014 Oct 01	-1.931 ± 0.085	1.93 ± 1.25	-0.999	0.028	2015 Aug 12	-1.914 ± 0.101	1.57 ± 1.49	-0.999	0.034
2014 Oct 19	-1.958 ± 0.075	2.24 ± 1.11	-0.999	0.024	2015 Sept 17	-1.944 ± 0.069	1.95 ± 1.01	-0.999	0.022
2015 June 22	-1.747 ± 0.142	-0.93 ± 2.10	-0.997	0.052					

Note. Slope and Intercept of $\log F_\nu$ against $\log \nu$, r – Pearson's coefficient and P – null hypothesis probability.

$\log \nu_{peak} = 15.5$ value from Chang et al. (2019), the 3HSP catalogue of extreme and high synchrotron peaked blazars. Physical parameters of the jet were estimated by Chen (2018) using SSC/Thomson model.

During imaging of host galaxies in *R* band the source remains unresolved, only historical $R = 15.99 \pm 0.03$ magnitude of the source core was recorded on 1998 December 16, by Nilsson et al.

(2003). This object is one of the three, from our monitoring, with the highest brightness changes of about 1.3 magnitude. The colour has tendencies to change during time of observations (about 0.3 mag). From colour–magnitude dependencies we can conclude that small BWB variations are present, which is one of the characteristics of BL Lac objects. During TJO monitoring one outburst was detected.

4.4 1212+467

The source was discovered in 1400 MHz Green Bank radio survey (Maslowski 1972). In Roma-BZCAT Multifrequency Catalogue of Blazars, it was classified as a FSRQ (Massaro et al. 2015). Its spectroscopic redshift was determined to be $z = 0.720154$ (Richards et al. 2015). Radio morphology of the source was found to be lobe-core-lobe (Kimball et al. 2011). In the catalogue of Spectral Properties of Quasars from SDSS DR14 (Rakshit et al. 2020) are available the logarithmic fiducial single-epoch black hole mass calculated based on Hβ, Mg II, and C IV lines (8.891813 ± 0.057461), and logarithmic Eddington ratio based on fiducial single-epoch black hole mass (-0.707690). The logarithm of ν_{peak} is estimated as 13.34 in Mao & Urry (2017). In paper (Krawczyk et al. 2015), it is given the spectral index difference (0.2) for the reddening law from Leighly et al. (2014).

The different values of V and R magnitudes were given in several catalogues. The $R = 17.13$ magnitude from catalogue of the CLASS blazar survey given by Marchã et al. (2001) is close to the minimum value which we observed. With designation LQAC $183 + 046\,007$ source participates in the 1st and the 2nd Large Quasar Astrometric Catalogue which is a compilation of all the recorded quasars (Souchay et al. 2009, 2012). From the 1st LQAC catalogue, $V = 17.77$ and $R = 17.42$ magnitudes are close to our average magnitudes. In the 2nd LQAC catalogue, only $V = 19.14$ magnitude was presented and this is the highest magnitude ever observed. In both bands the brightness changes by about 0.8 magnitude, from 2013 to 2019. The slope and Pearson's coefficient of colour–time and colour–magnitude dependencies are almost 0 with probability greater than 0.95. Colour values are in range of about 0.3 mag, around averaged value. We can not say that even tendencies are present because the slope and Pearson's coefficient are close to 0, but with probability less than 0.95, we can say that this object shows nearly achromatic behaviour.

4.5 1242+574

The source was catalogued for the first time in the 87 GB catalogue (Gregory & Condon 1991). In the 12th edition of a catalogue of quasars and active nuclei, it was classified as BL Lac (Véron-Cetty & Véron 2006). Its spectroscopy redshift $z = 0.99822855$ was estimated (Richards et al. 2015). The source $\nu_{peak} = 14.35$ Hz in the observed frame (νf_ν), so is an ISP blazar (e.g. Ackermann et al. 2011; Mao & Urry 2017). The source is in 1st and 3rd *Fermi*-LAT catalogues of sources above 10 GeV (Ackermann et al. 2013; Acero et al. 2015). In the MST catalogue of γ-ray source candidates above 10 GeV the source has designation 9Y-MST J1244+5709 (Campana, Massaro & Bernieri 2018).

In both bands, the brightness change is 0.8 magnitude. Similarly as object 1212+467, we can say that this object shows nearly achromatic behaviour. The slope and Pearson's coefficient of colour–time and colour–magnitude dependencies are negative, close to 0 and probability is greater than 0.05 and less than 0.95. The colour has tendencies to change during time of observations (almost 0.4 mag).

4.6 1429+249

The source was discovered in second MIT–Green Bank 5 GHz radio survey (Langston et al. 1990). With broad Balmer and other permitted lines in spectra, it was classified as a type 1 Seyfert galaxy in paper (Véron-Cetty & Véron 2006), and with general spectroscopic characteristics in paper (Sexton et al. 2022). In an all sky catalog

of γ-ray blazars, the source was classified as a dual nature of both BL Lac as well as FSRQ (D'Abrusco et al. 2014). Its spectroscopic redshift was determined to be $z = 0.40659$ (Lehner et al. 2018). In the paper Rakshit et al. (2020) were provided the logarithmic black hole mass (8.658600 ± 0.027332), and logarithmic Eddington ratio (-0.853556), both calculated based on Hβ, Mg II, and C IV lines. Absolute i band magnitude is -24.134 from (Condon et al. 2013). The spectral index difference of 0.006 is given in paper (Krawczyk et al. 2015).

The source is known also as LQAC $217 + 024\,010$. In the 1st LQAC catalogue were given $V = 16.09$, and $R = 17.43$ magnitudes, and in the 2nd LQAC $V = 17.68$ and $R = 17.44$ (Souchay et al. 2009, 2012). The V from the 1st catalogue is lower than in R band (authors), and the remained values are out of range of our observed magnitudes. The brightness of the source changed by 0.5 and 0.3 magnitude during six years in V and R band, respectively. Abbé's and F statistics for this object are close to the critical values. Abbé's criterion shows that the object has systematic variations in relations to comparison star A in V band, and to both stars in R band. F-test shows that the object is variable only in V band. From the colour–magnitude relations we can say that the BWB variations are present.

4.7 1535+231

The authors of papers Arp (2001) and Arp et al. (2001) claim that the object is correlated to the nearby active galaxy Arp 220[3] ($z = 0.018$) and most likely has been ejected from it, even the object is at 43.1 arcmin distance from the galaxy, and has higher redshift ($z = 0.4627$). Again in 2015 the redshift was determined by spectroscopy $z = 0.462515$, in Richards et al. (2015), when the object was classified as QSO. Based on mid-infrared colours of Wide-Field Infrared Survey Explorer the source was classified as mixed BL Lac and FSRQ blazar (D'Abrusco et al. 2019). The source was classified according to its general spectroscopic characteristics as type 1 Seyfert galaxy in paper Sexton et al. (2022). The logarithmic black hole mass (8.399292 ± 0.047624), and logarithmic Eddington ratio (-0.932017), both were calculated based on Hβ, Mg II, and C IV lines, were provided in the paper Rakshit et al. (2020). The spectral index difference according to Krawczyk et al. (2015) is 0.024.

In both bands, the brightness changed by about 0.9 magnitudes. The colour changed during time of observations almost a half magnitude. In case of colour–magnitude relations we can not say that RWB variations are present, only the RWB tendencies are present because the probability is greater than 0.05. This object is the faintest (average magnitudes are greater than 18 mag in both filters), which differs from the historical $V = 17.7$ given in Véron-Cetty & Véron (2001).

4.8 1556+335

The source was detected for the first time during NRAO 5 GHz radio survey of faint sources, which was initiated in 1967 and presented in Davis (1971). It was identified as QSO by Wills & Wills (1979), later as FSRQ by Massaro et al. (2015) in the 5th edition of the Roma-BZCAT Multifrequency Catalogue of Blazars. The first spectroscopic redshift $z = 1.65$ by Wills & Wills (1979) is similar to the one later determined by Richards et al. (2015), $z = 1.653598$. The presence of two absorption complexes in the spectrum could be explained with one of two models: one in which the source is directly

---

[3] Also known as IC 4553 – galaxy merging system with two nuclei.

responsible for velocities seen in both complexes, and the second in which complexes are related with two clusters, one cluster contains the source, while the other one is in the line of sight (Morris et al. 1986). The source radio morphology class was defined as *core* – a quasar with radio emission only at the optical position, in Kimball et al. (2011). Using spectral properties of quasar the logarithmic black hole mass (10.024996 ± 0.046142), and logarithmic Eddington ratio (-0.874986), were provided in the paper Rakshit et al. (2020). The ν_{peak} is 13.92 (Mao & Urry 2017).

During our monitoring the object is variable only in *V* band in relation to star A. This is the most stable object from our list. The historical $V = 17$ magnitude, the lowest ever detected, was given in catalogue Hewitt & Burbidge (1987), and $R = 16.94$ (for 1996.523) in paper Helfand et al. (2001) is close to the average magnitude which we observed. For six years the brightness decreased by 0.2 mag in both bands. From the colour–time and colour–magnitude dependencies we can conclude that colour had not changed during time and that the achromatic behaviour is present.

4.9 1607+604

After NRAO 4.85 GHz survey the source was catalogued by Gregory & Condon (1991) and Becker et al. (1991) in second paper source was marked as extended. The redshift and classification as RL quasar are obtained by spectroscopy in Laurent-Muehleisen et al. (1998). The authors of D'Abrusco et al. (2014) classified the object as BL Lac. The radio and optical cross-identification of the source was accomplished by authors of paper Bauer et al. (2000). They presented the source redshift $z = 0.178$, and radio emission as extended and resolved into three components.

During time of observations the brightness changes by 0.5 and 0.4 magnitudes in *V* and *R* bands, respectively. The colour has tendencies to change by about 0.4 mag. In case of colour–magnitude relations we can say that BWB variations are present.

4.10 1612+378

In the 5th edition of the Roma-BZCAT Multifrequency Catalogue of Blazars the source was classified as FSRQ. The redshift $z = 1.531239$ determined by spectroscopy was given in Richards et al. (2015). Absolute *i* magnitude of -28.332 mag is obtained in paper Rafiee & Hall (2011). As 1556+335, the radio morphology was classified as *core* in Kimball et al. (2011) and the logarithmic black hole mass (9.684895 ± 0.084033), and logarithmic Eddington ratio (-0.454582), were provided in the paper Rakshit et al. (2020). The source is ISP, its synchrotron peak frequency is $log\nu_{peak} = 14.16$, derived in Mao & Urry (2017).

In both bands, amplitudes of the brightness changes are 0.4 mag. The amplitude of colour changes is about 0.2 mag. In case of colour–magnitude relations we can say that BWB variations are present, which is one of the characteristics of BL Lac objects.

4.11 1722+119

This is one of the first discovered BL Lac objects. For the first time it appeared in the fourth Uhuru catalogue of X-ray sources Forman et al. (1978). After a decade the object was independently classified as BL Lac, and its redshift estimation was given in papers Griffiths et al. (1989) $z = 0.018$, and Brissenden et al. (1990) $z > 0.1$, and historical magnitude was $V = 16.6$ mag on 1979, Griffiths et al. (1989). In Ahnen et al. (2016) new redshift was given 0.34 ± 0.15. The object is the one of the sources detected with MAGIC in TeV, announced

Table 11. The colour – magnitude dependencies for 1722+119.

Source	Slope	Intercept	r	P
Before 2016	− 0.051 ± 0.018	1.21 ± 0.28	− 0.32	0.1510
After 2016	0.034 ± 0.006	− 0.08 ± 0.08	0.64	0.0012

Note. r – Pearson's coefficient and P – null hypothesis probability.

by Cortina (2013). The MAGIC observations were triggered by the optical outburst on 2013 May when the *R*-band magnitude reached 14.65 mag which was the biggest ever observed since 2005, when the Tuorla blazar monitoring programme started. According to the position of the synchrotron peak frequency object is HSP confirmed by Nieppola et al. (2006), Ackermann et al. (2011), and Chang et al. (2019). Chang et al. (2019) included this source in the third catalogue of extremely and high-synchrotron peaked blazars, with $log\nu_{peak} = 15.7$. Jet properties of source were analysed but only the core temperature was obtained to be higher than 10.7 K in Lister et al. (2011), its physical parameters were estimated by Chen (2018) using SSC/Klein–Nishina model.

During 2008 – 2012, variability in *R* band was present, but $B − R$ chromatism in the ~1 magnitude range of *R* band has not been revealed, in Wierzcholska et al. (2015). Since 2011 the authors of Taris et al. (2016) investigated the long term periodicity in *V* and *R* bands using Lomb–Scargle method and CLEANEST algorithm (Roberts, Lehar & Dreher 1987). Period was discovered only in *R* band of 432 d with Lomb–Scargle method, and 435.7 d with CLEANEST algorithm. In Taris et al. (2018) was detected period of 35 d of variability in optical *G* band, for period of observations from 2013 to 2016. In June 2015 during three hours of monitoring, object did not show the variability in *V* band, showed possible variability in *R* band, and a strong RWB trend of the optical spectrum (Kalita, Gupta & Gu (2021)). The authors of paper Lindfors et al. (2016) discovered correlation between optical *R* band and radio light curves at 15 GHz. Brightness variability in data collected over 12 yr in *X*-ray was analysed by Rani, Wiita & Gupta (2009). The period of about one year was explained as observational artefact.

With almost 2 magnitude changes in brightness this object has the highest brightness changes. In the *R* band has the maximum brightness 14.371 mag on the date 2016 August 28 (this period was not covered with observations in *V* band), the next maximum of 14.458 mag occurred on 2018 July 20, and was detected in *V* band of 14.888 mag. The slope and Pearson's coefficient of colour–time is positive, but close to 0, with a probability close to 0.9. The slope of the colour–magnitude dependencies is around 0, Pearson's coefficient is positive. The colour has small tendencies to change during time of observations. From colour–magnitude dependencies we can conclude that BWB variations are present, but we noted that during observational period two tendencies of colour variation in dependence of *R* magnitude are present. One in the beginning of observations from 2013 to 2016, and the second from 2016 to the end of observational cycle. If we separate the data in two sections in first three years RWB tendencies, and in the next three years period BWB variations were present, see Table 11 and Fig. 8. In the second period were detected both minimum and maximum of object brightness. In the last 300 d brightness decreased by 1.6 magnitude, and reached the minimum 16.8 and 16.3 mag in *V* and *R* band, respectively.

4.12 1741+597

The source was catalogued in the same year in two papers Gregory & Condon (1991) and Becker et al. (1991). In Laurent-Muehleisen
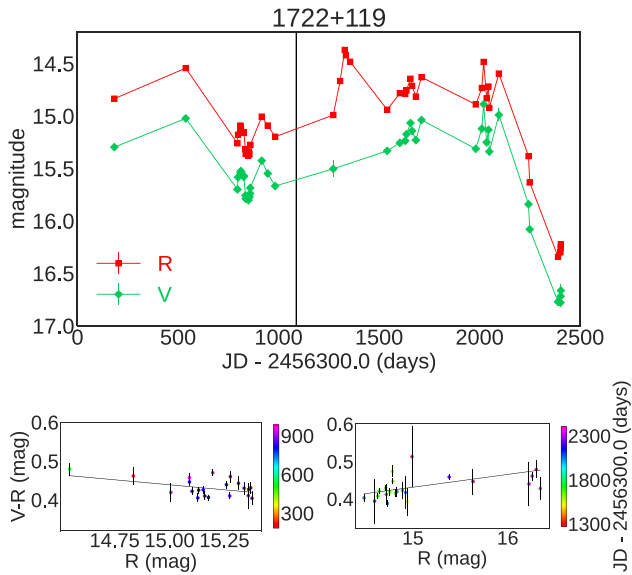
Figure 8. Light curve of 1722+119; colour–magnitude diagrams 2013 – 2016 (left-bottom), and 2016 – 2019 (right-bottom).

et al. (1998) the source was classified as BL Lac. The redshift was determined by photometry $z = 0.415$ by Richards et al. (2009). The source is ISP according to papers Nieppola et al. (2006) and Ackermann et al. (2011). We adopt $log\nu_{peak} = 15.20$ given in Mao & Urry (2017) and classify source as HPS. With the name 9Y-MST J1742+5946 source is in the MST catalogue of γ-ray source candidates above 10 GeV (Campana et al. 2018). In Chen (2018) are estimated physical parameters of jet using SSC/Thomson model.

The host galaxy was detected by Nilsson et al. (2003), the *R*-band magnitude of nucleus (17.06 ± 0.03) and host galaxy (19.33 ± 0.06) with effective radius of 1.6 ± 0.2 arcsec were presented in the paper. This source is the second one with respect to the brightness change, with about 1.6 mag. In the last 250 d object became brighter by 1.2 magnitude. The colour has tendencies to change during time of observations, these changes are about 0.3 mag. From colour–magnitude dependencies we can conclude that BWB variations are present.

5 DISCUSSIONS AND CONCLUSIONS

To understand the emission mechanism of blazars on diverse time-scales, flux variability study play an important role and can provide the information about emitting region, for example, size, location, and its dynamics (Ciprini et al. 2003). Variability in blazars can be of intrinsic as well as of extrinsic nature. The extrinsic variability in blazars is caused by frequency-dependent interstellar scintillation and is found to be dominant mechanism in low-frequency radio observations (Wagner & Witzel 1995). Intrinsic mechanism operates across whole EM spectrum and include directly those causing variation in the jet emission. In blazars, the Doppler boosted non-thermal radiation from the jet dominates on the thermal emission from the accretion disc (e.g. Chakrabarti & Wiita 1993; Mangalam & Wiita 1993; Urry & Padovani 1995; Wagner & Witzel 1995; Ulrich et al. 1997; Blandford, Meier & Readhead 2019, and references therein). On diverse time-scales such as IDV, STV, and LTV variability in blazars can be explained by various jet based models, for example, shock-in-jet, turbulence behind the shock, or other irregularities in the jet flow produced by variations in the outflow parameters (e.g.

Blandford & Königl 1979; Marscher & Gear 1985; Bhatta et al. 2013; Marscher 2014; Calafut & Wiita 2015, and references therein). Variation in the jet geometry due to changing jet direction may lead to the variations in the Doppler factor and Lorentz factor of the relativistic blobs moving along the jet, which in turn can lead to STV and LTV in the blazar (Hovatta et al. 2009). During the low flux states of blazars, the variability can be attributed to accretion disc instabilities since thermal radiation from the central region of blazars may dominate over jet emission (Chakrabarti & Wiita 1993; Mangalam & Wiita 1993).

The variation of Doppler factor can cause slight deviation in the optical spectra of the blazar from a power law which leads to a BWB trend (Villata et al. 2006). The increase in brightness of the blazar due to injection of fresh electrons with an energy distribution harder than that of the previously cooled ones can also cause BWB trend (Kirk, Rieger & Mastichiadis 1998; Mastichiadis & Kirk 2002). A RWB trend indicates an increase of thermal contribution at the blue end of the spectrum, with decrease in non-thermal jet emission (Villata et al. 2006; Gaur, Gupta & Wiita 2012a). The presence of both BWB and RWB trends in some blazars can be explained by superposition of both blue and red emission components where the redder one is attributed to the synchrotron radiation from the relativistic jet while the blue component could come from the thermal emission from the accretion disc.

In this paper, we analysed the multiband optical photometric data of 12 blazars selected from a sample of 47 AGNs detected by Bourda et al. (2011). Among these 12 blazars: 6 are BL Lacs, 4 are FSRQs, and 2 show dual nature of BL Lac/FSRQ. During 2013 April 14 – 2019 August 08, the optical photometric observations of these blazars were carried out in *V* and *R* passbands using 8 telescopes located in 4 countries in Europe. In our ∼ six years of observations, most of the blazars have shown significant flux and colour variations on STV and LTV time-scales, and the variability pattern in *V* and *R* bands found to be similar. On the LTV time-scale, the minimum variation of ∼ 0.2 mag is found in the blazar 1556+335 while the maximum variation of ∼ 2.0 mag is found in two blazars, namely 1722+119 and 1741+597. Four BL Lacs, two FSRQs and one blazar with dual nature show BWB trend. RWB trend is displayed by one BL Lac and one blazar with dual nature. The BL Lac 1722+119 shows RWB trend in the first about three years of observations, and BWB trend in the next about three years of observations. These trends show that in our sample of blazars and their observations, the most commonly found trends, for example, BWB in BL Lacs and RWB in FSRQs (e.g. Gu et al. 2006; Gaur et al. 2012b; Gupta et al. 2017b, and references therein) were not always found. In future, we plan observations of more densely sampled light curves for extended period of time for these as well as several other blazars to make a better conclusion on BWB and RWB trends of BL Lacs and FSRQs.

ACKNOWLEDGEMENTS

6 DATA AVAILABILITY

The light curves presented in this paper will be published in the electronic version of the Journal and in the CDS Vizier service, with the form illustrated in Table 3.

REFERENCES

Abdo A. A., et al., 2010, ApJ, 716, L30
Abolfathi B., et al., 2018, ApJS, 235, 42
Abrahamyan, H. V. (Jun 2019) Optical variability of blazars Astronomische Nachrichten, Volume 340, Issue 5, pp. 437-444, ,
Acero F., et al., 2015, ApJS, 218, 23
Ackermann M., et al., 2011, ApJ, 743, L171
Ackermann M., et al., 2013, ApJS, 209, 34
Ahnen M. L., et al., 2016, MNRAS, 459, 3271
Arp H. C., Burbidge E. M., Chu Y., Zhu X., 2001, ApJ, 553, L11
Arp H., 2001, ApJ, 549, L780
Bauer F. E., Condon J. J., Thuan T. X., Broderick J. J., 2000, ApJS, 129, 547
Becker R. H., White R. L., Edwards A. L., 1991, ApJS, 75, 1
Bessell M. S., Castelli F., Plez B., 1998, A&A, 333, 231
Bhatta G., 2021, ApJ, 923, L7
Bhatta G., et al., 2013, A&A, 558, 92
Bhatta G., Zola S., Drozdz M., Reichart D., Haislip J., Kouprianov V., Matsumoto K., et al., 2023, MNRAS, 520, 2633
Blandford R. D., Königl A., 1979, ApJ, 232, L34
Blandford R., Meier D., Readhead A., 2019, ARA&A, 57, 467
Böttcher M., 2007, Ap&SS, 309, 95
Bourda G., Charlot P., Porcas R. W., Garrington S. T., 2010, A&A, 520, 113
Bourda G., Collioud A., Charlot P., Porcas R., Garrington S., 2011, A&A, 526, 102
Brissenden R. J. V., Remillard R. A., Tuohy I. R., Schwartz D. A., Hertz P. L., 1990, ApJ, 350, L578
Calafut V., Wiita P. J., 2015, JA&A, 36, 255
Campana R., Massaro E., Bernieri E., 2018, A&A, 619, 23
Chakrabarti S. K., Wiita P. J., 1993, ApJ, 411, L602
Chang Y. L., Arsioli B., Giommi P., Padovani P., 2017, A&A, 598, 17
Chang Y. L., Arsioli B., Giommi P., Padovani P., Brandt C. H., 2019, A&A, 632, 77
Charlot P., et al., 2020, A&A, 644, 159
Chavira E., 1959, Boletin de los Observatorios Tonantzintla y Tacubaya, 2, 3
Chen L., 2018, ApJS, 235, 39
Chonis T. S., Gaskell C. M., 2008, AJ, 135, 264
Ciprini S., Tosti G., Raiteri C. M., Villata M., Ibrahimov M. A., Nucciarelli G., Lanteri L., 2003, A&A, 400, 487
Condon J. J., Kellermann K. I., Kimball A. E., Ivezić Ž., Perley R. A., 2013, ApJ, 768, L37
Cortina J., 2013, ATel, 5080, 1
D'Abrusco R., et al., 2019, ApJS, 242, 4
D'Abrusco R., Massaro F., Paggi A., Smith H. A., Masetti N., Landoni M., Tosti G., 2014, ApJS, 215, 14
Damljanović G., Taris F., Jovanović M. D., 2020, in Bizouard C., ed., Proceedings of the Journées 2019, Observatoire de Paris, Paris, France, 7-9 October 2019. Astrometry, Earth Rotation, and Reference Systems in the GAIA era, p. 21
Davis M. M., 1971, AJ, 76, 980
de Diego J. A., 2010, AJ, 139, 1269
de Vries W. H., Becker R. H., White R. L., Helfand D. J., 2004, AJ, 127, 2565
Dong X. Y., et al., 2018, AJ, 155, 189
Doroshenko V. T., Efimov Y. S., Borman G. A., Pulatova N. G., 2014, Astrophysics, 57, 176
Fan J. H., et al., 2016, ApJS, 226, 20
Feissel-Vernier M., 2003, A&A, 403, 105
Forman W., Jones C., Cominsky L., Julien P., Murray S., Peters G., Tananbaum H., Giacconi R., 1978, ApJS, 38, 357
Fossati G., Maraschi L., Celotti A., Comastri A., Ghisellini G., 1998, MNRAS, 299, 433
Gaia Collaboration, et al., 2022, preprint (arXiv:2208.00211)
Gattano C., Lambert S. B., Le Bail K., 2018, A&A, 618, 80
Gaur H., et al., 2012b, MNRAS, 425, 3002
Gaur H., Gupta A. C., Wiita P. J., 2012a, AJ, 143, 23
Gopal-Krishna, Sagar R., Wiita P. J., 1993, MNRAS, 262, 963
Gregory P. C., Condon J. J., 1991, ApJS, 75, 1011
Griffiths R. E., Wilson A. S., Ward M. J., Tapia S., Ulvestad J. S., 1989, MNRAS, 240, 33
Gu M. F., Ai Y. L., 2011, A&A, 528, 95
Gu M. F., Lee C. U., Pak S., Yim H. S., Fletcher A. B., 2006, A&A, 450, 39
Gupta A. C., Banerjee D. P. K., Ashok N. M., Joshi U. C., 2004, A&A, 422, 505
Gupta A. C., et al., 2017a, MNRAS, 465, 4423
Gupta A. C., et al., 2017b, MNRAS, 472, 788
Hald A., 1952, Statistical theory with engineering applications. Wiley, New York–London
Harris D. E., Forman W., Gioa I. M., Hale J. A., Harnden F. R., Jones C., Karakashian T. et al., 1996, VizieR Online Data Catalog: The 2E Catalogue (Harris+ 1994), IX/13
Healey S. E., Romani R. W., Taylor G. B., Sadler E. M., Ricci R., Murphy T., Ulvestad J. S., Winn J. N., 2007, ApJS, 171, 61
Heidt J., Wagner S. J., 1996, A&A, 305, 42
Helfand D. J., Stone R. P. S., Willman B., White R. L., Becker R. H., Price T., Gregg M. D., McMahon R. G., 2001, AJ, 121, 1872
Hewett P. C., Foltz C. B., Chaffee F. H., 1995, AJ, 109, 1498
Hewitt A., Burbidge G., 1987, ApJS, 63, 1
Hodge J. A., Becker R. H., White R. L., Richards G. T., 2013, ApJ, 769, L125
Hovatta T., Valtaoja E., Tornikoski M., Lähteenmäki A., 2009, A&A, 494, 527
Isler J. C., Urry C. M., Coppi P., Bailyn C., Brady M., MacPherson E., Buxton M., Hasan I., 2017, ApJ, 844, L107
Jovanović M. D., 2019, Serbian Astronomical Journal, 199, 55
Jovanović M. D., Damljanović G., 2020, Bulgarian Astronomical Journal, 33, 38
Jovanović M. D., Damljanović G., Cvetković Z., Pavlović R., Stojanović M., 2020, Publications of the Astronomical Society 'Rudjer Boskovic', 20, 23

Jovanović M. D., Damljanović G., Taris F., 2021, in XIX Serbian Astronomical Conference, Publ. Astron. Obs. Belgrade No. 100, p. 253–258

Jovanović M. D., Damljanović G., Taris F., 2023, Publications of the Astronomical Society 'Rudjer Boskovic', 24

Jovanovic M. D., Damljanovic G., Vince O., 2018, in Proceedings of the XI Bulgarian-Serbian Astronomical Conference, Publ. Astron. Soc. "Rudjer Bošković" No 18, p. 197–205

Jun H. D., Im M., 2013, ApJ, 779, L104

Kalita N., Gupta A. C., Gu M., 2021, ApJS, 257, 41

Kimball A. E., Ivezić Ž., Wiita P. J., Schneider D. P., 2011, AJ, 141, 182

Kirk J. G., Rieger F. M., Mastichiadis A., 1998, A&A, 333, 452

Krawczyk C. M., Richards G. T., Gallagher S. C., Leighly K. M., Hewett P. C., Ross N. P., Hall P. B., 2015, AJ, 149, 203

Langston G. I., Heflin M. B., Conner S. R., Lehar J., Carilli C. L., Burke B. F., 1990, ApJS, 72, 621

Laurent-Muehleisen S. A., Kollgaard R. I., Ciardullo R., Feigelson E. D., Brinkmann W., Siebert J., 1998, ApJS, 118, 127

Lehner N., Wotta C. B., Howk J. C., O'Meara J. M., Oppenheimer B. D., Cooksey K. L., 2018, ApJ, 866, L33

Leighly K. M., Terndrup D. M., Baron E., Lucy A. B., Dietrich M., Gallagher S. C., 2014, ApJ, 788, L123

Lemeshko S., 2006, Measurement Techniques, 49, 962

Lindfors E. J., et al., 2016, A&A, 593, 98

Lister M. L., et al., 2011, ApJ, 742, L27

Malkin Z. M., 2013, Astron. Rep., 57, 128

Mangalam A. V., Wiita P. J., 1993, ApJ, 406, L420

Mao P., Urry C. M., 2017, ApJ, 841, L113

Marcha M. J. M., Browne I. W. A., Impey C. D., Smith P. S., 1996, MNRAS, 281, 425

Marchã M. J., Caccianiga A., Browne I. W. A., Jackson N., 2001, MNRAS, 326, 1455

Marscher A. P., 2014, ApJ, 780, L87

Marscher A. P., Gear W. K., 1985, ApJ, 298, L114

Maslowski J., 1972, AcA, 22, 227

Massaro E., Maselli A., Leto C., Marchegiani P., Perri M., Giommi P., Piranomonte S., 2015, Ap&SS, 357, 75

Mastichiadis A., Kirk J. G., 2002, PASA, 19, 138

Meusinger H., Hinze A., de Hoon A., 2011, A&A, 525, 37

Miller H. R., Carini M. T., Goodrich B. D., 1989, Nature, 337, 627

Morris S. L., Weymann R. J., Foltz C. B., Turnshek D. A., Shectman S., Price C., Boroson T. A., 1986, ApJ, 310, L40

Nass P., Bade N., Kollgaard R. I., Laurent-Muehleisen S. A., Reimers D., Voges W., 1996, A&A, 309, 419

Nieppola E., Tornikoski M., Valtaoja E., 2006, A&A, 445, 441

Nilsson K., Pursimo T., Heidt J., Takalo L. O., Sillanpää A., Brinkmann W., 2003, A&A, 400, 95

Pininti V. R., Bhatta G., Paul S., Kumar A., Rajgor A., Barnwal R., Gharat S., 2023, MNRAS, 518, 1459

Pukelsheim F., 1994, The American Statistician, 48, 88

Rafiee A., Hall P. B., 2011, ApJS, 194, 42

Rakshit S., Stalin C. S., Kotilainen J., 2020, ApJS, 249, 17

Rani B., Wiita P. J., Gupta A. C., 2009, ApJ, 696, L2170

Razali N. M., Wah Y. B., et al., 2011, J. Stat. Model. Anal., 2, 21

Richards G. T., et al., 2009, ApJS, 180, 67

Richards G. T., et al., 2015, ApJS, 219, 39

Roberts D. H., Lehar J., Dreher J. W., 1987, AJ, 93, 968

Schlafly E. F., Finkbeiner D. P., 2011, ApJ, 737, L103

Sexton R. O., Secrest N. J., Johnson M. C., Dorland B. N., 2022, ApJS, 260, 33

Souchay J., Andrei A. H., Barache C., Bouquillon S., Suchet D., Taris F., Peralta R., 2012, A&A, 537, 99

Souchay J., et al., 2009, A&A, 494, 799

Spano M., Mowlavi N., Eyer L., Burki G., Marquette J. B., Lecoeur-Taïbi I., Tisserand P., 2011, A&A, 536, 60

Stickel M., Padovani P., Urry C. M., Fried J. W., Kuehr H., 1991, ApJ, 374, L431

Strunov V., 2006, Measurement Techniques, 49, 755

Taris F., Andrei A., Roland J., Klotz A., Vachier F., Souchay J., 2016, A&A, 587, 112

Taris F., Damljanovic G., Andrei A., Souchay J., Klotz A., Vachier F., 2018, A&A, 611, 52

Tody D., 1986, in Crawford D. L., ed., Proceedings Volume 0627. Society of Photo-Optical Instrumentation Engineers (SPIE) Conference Series Vol. 627, Instrumentation in astronomy VI, p. 733

Tody D., 1993, in Hanisch R. J., Brissenden R. J. V., Barnes J., eds, Astronomical Society of the Pacific Conference Series Vol. 52. Astronomical Data Analysis Software and Systems II, p. 173

Ulrich M.-H., Maraschi L., Urry C. M., 1997, ARA&A, 35, 445

Urry C. M., Padovani P., 1995, PASP, 107, 803

van Dokkum P. G., 2001, PASP, 113, 1420

Véron-Cetty M. P., Véron P., 2001, A&A, 374, 92

Véron-Cetty M. P., Véron P., 2006, A&A, 455, 773

Villata M., et al., 2006, A&A, 453, 817

von Montigny C., et al., 1995, ApJ, 440, L525

Wagner S. J., Witzel A., 1995, ARA&A, 33, 163

Wierzcholska A., Ostrowski M., Stawarz Ł., Wagner S., Hauser M., 2015, A&A, 573, 69

Wills B. J., Wills D., 1979, ApJS, 41, 689

Zaječek M., et al., 2019, A&A, 630, 83

7 SUPPORTING INFORMATION

Supplementary data are available at *MNRAS* online.

Table 3. Examples of observations from 2013 to 2019 in *V* and *R* bands.

Please note: Oxford University Press is not responsible for the content or functionality of any supporting materials supplied by the authors. Any queries (other than missing material) should be directed to the corresponding author for the article.

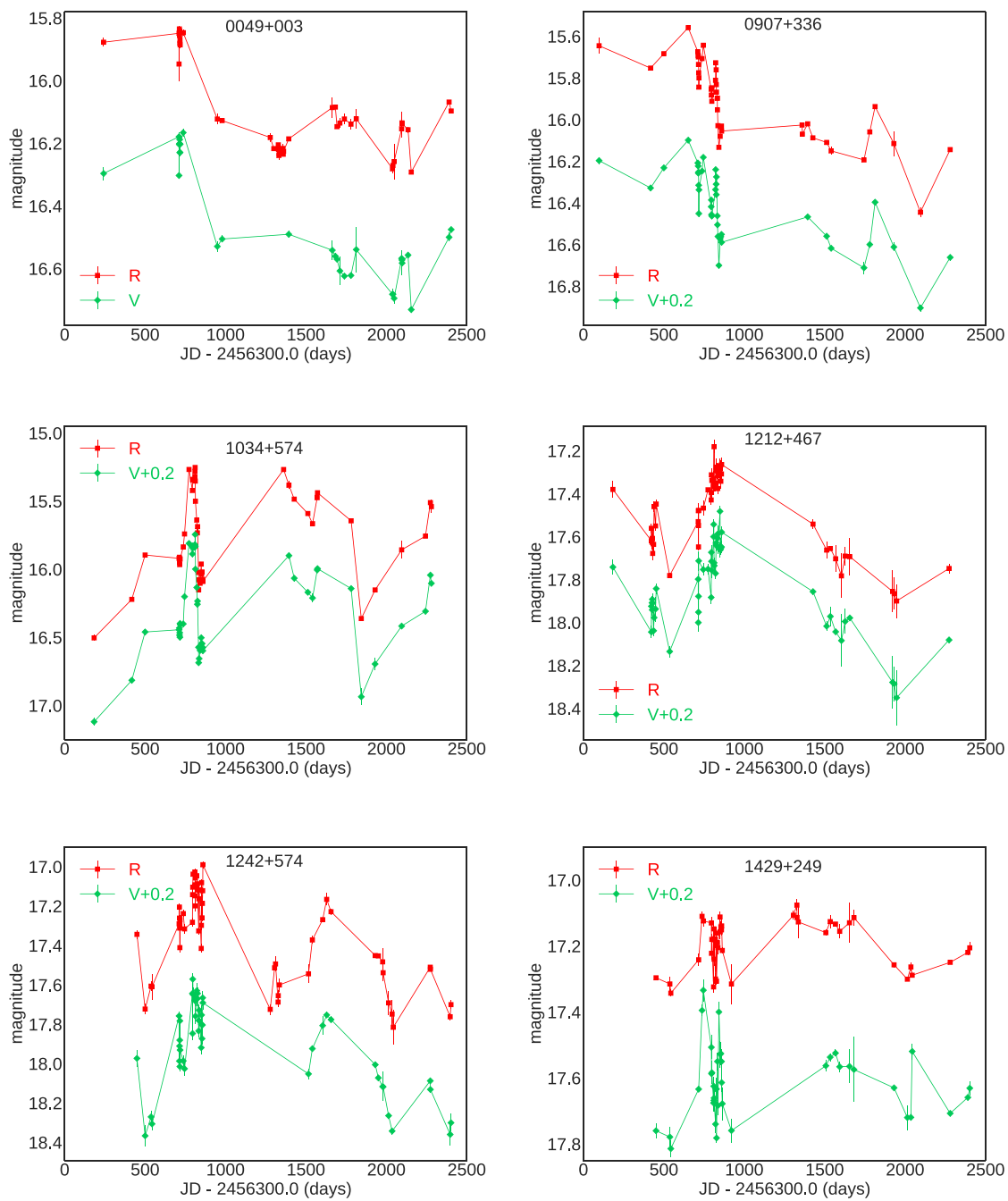## APPENDIX A: LIGHT CURVES OF *V* AND *R* BAND

Figure A1. Light curves of sources: 0049+003, 0907+336, 1034+574, 1212+467, 1242+574, 1429+249, 1535+231, 1556+335, 1607+604, 1612+378, 1722+119, and 1741+597.
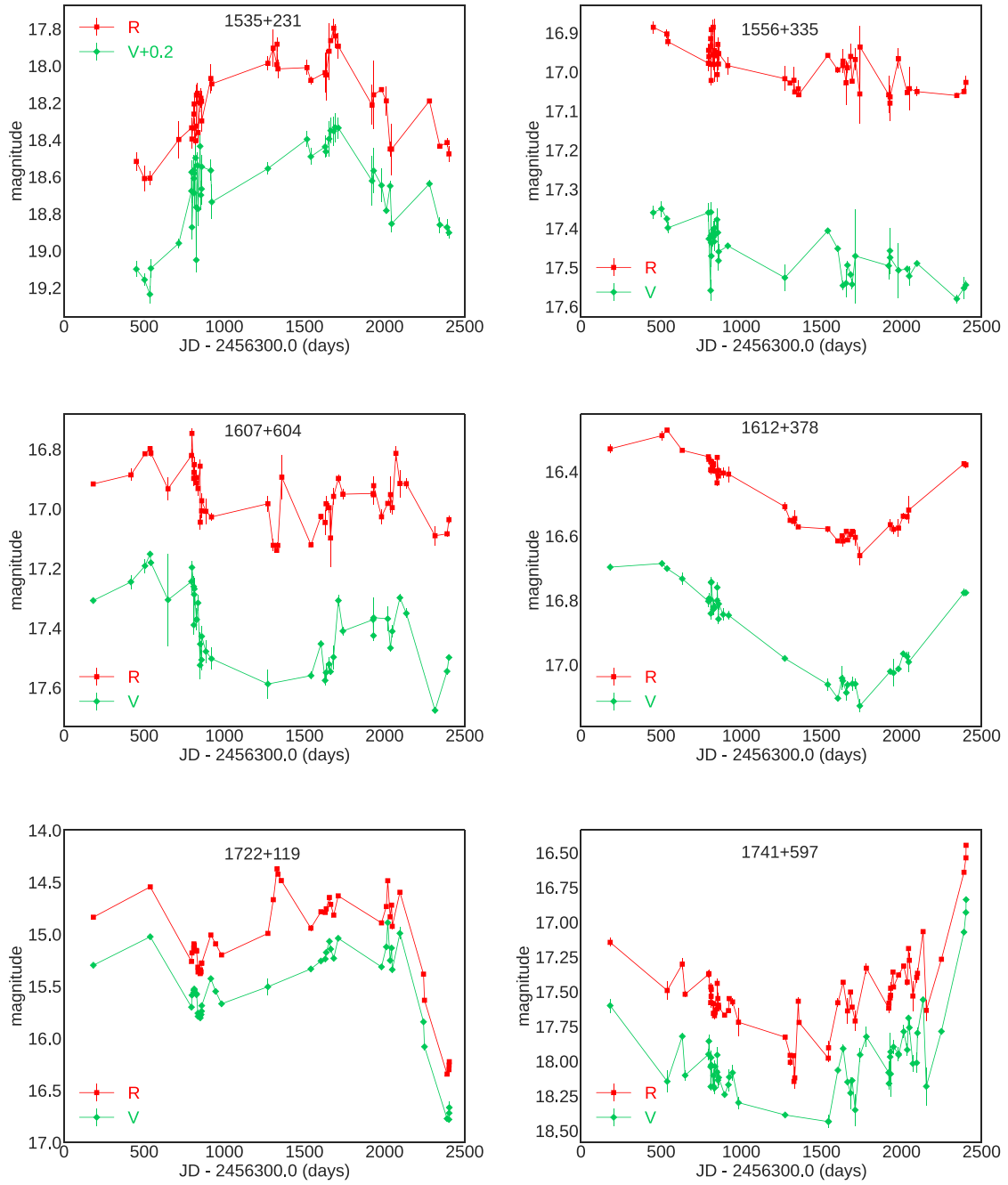
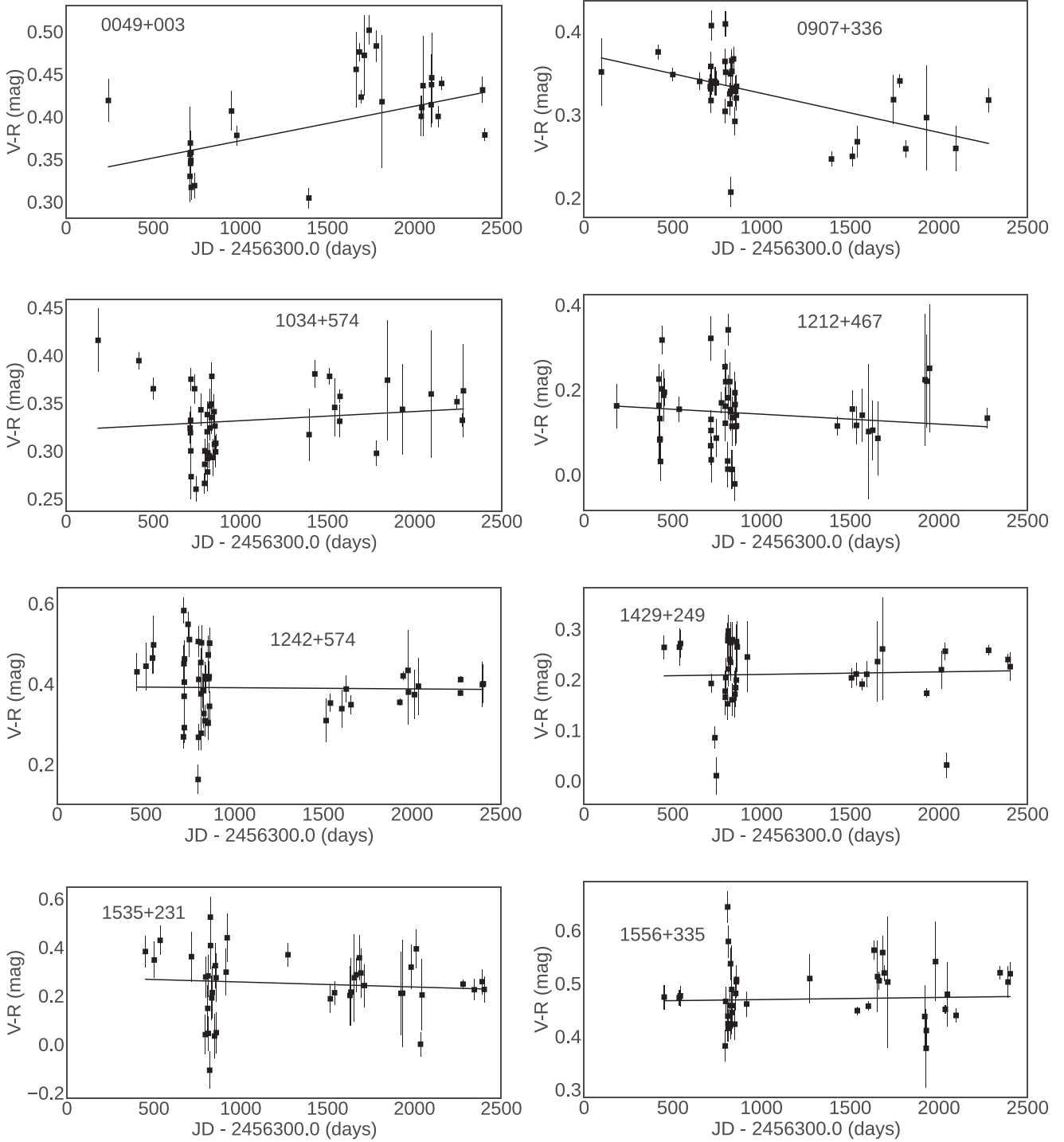**Figure A1.** *continued.*

APPENDIX B: LIGHT CURVES OF COLOUR INDICES $V - R$ VARIABILITY DURING TIME

Figure B1. The light curves of colour indices $V - R$ variability during period 2013 April – 2019 August of sources: 0049+003, 0907+336, 1034+574, 1212+467, 1242+574, 1429+249, 1535+231, 1556+335, 1607+604, 1612+378, 1722+119, and 1741+597. Details of all sources can be found in Table 5.
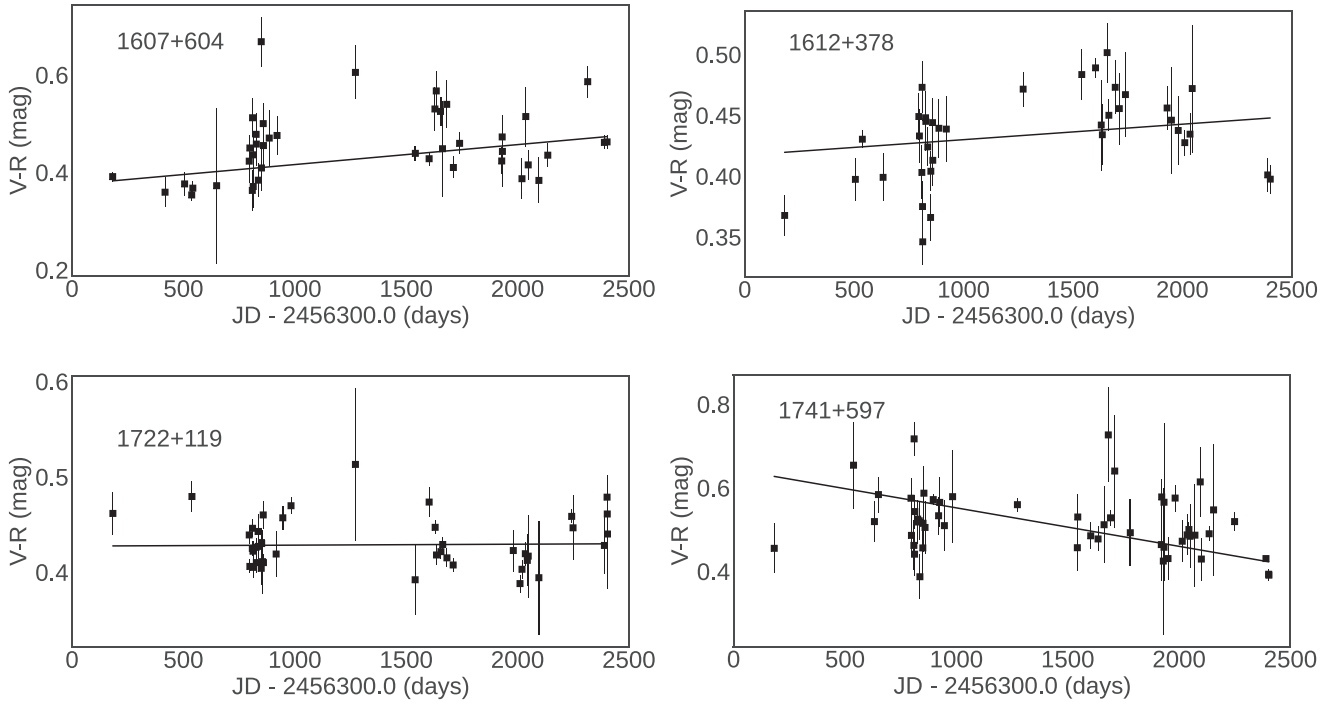
Figure B1. *continued.*

APPENDIX C: THE CORRELATION BETWEEN COLOUR INDICES *V – R* AND *R*-BAND MAGNITUDE
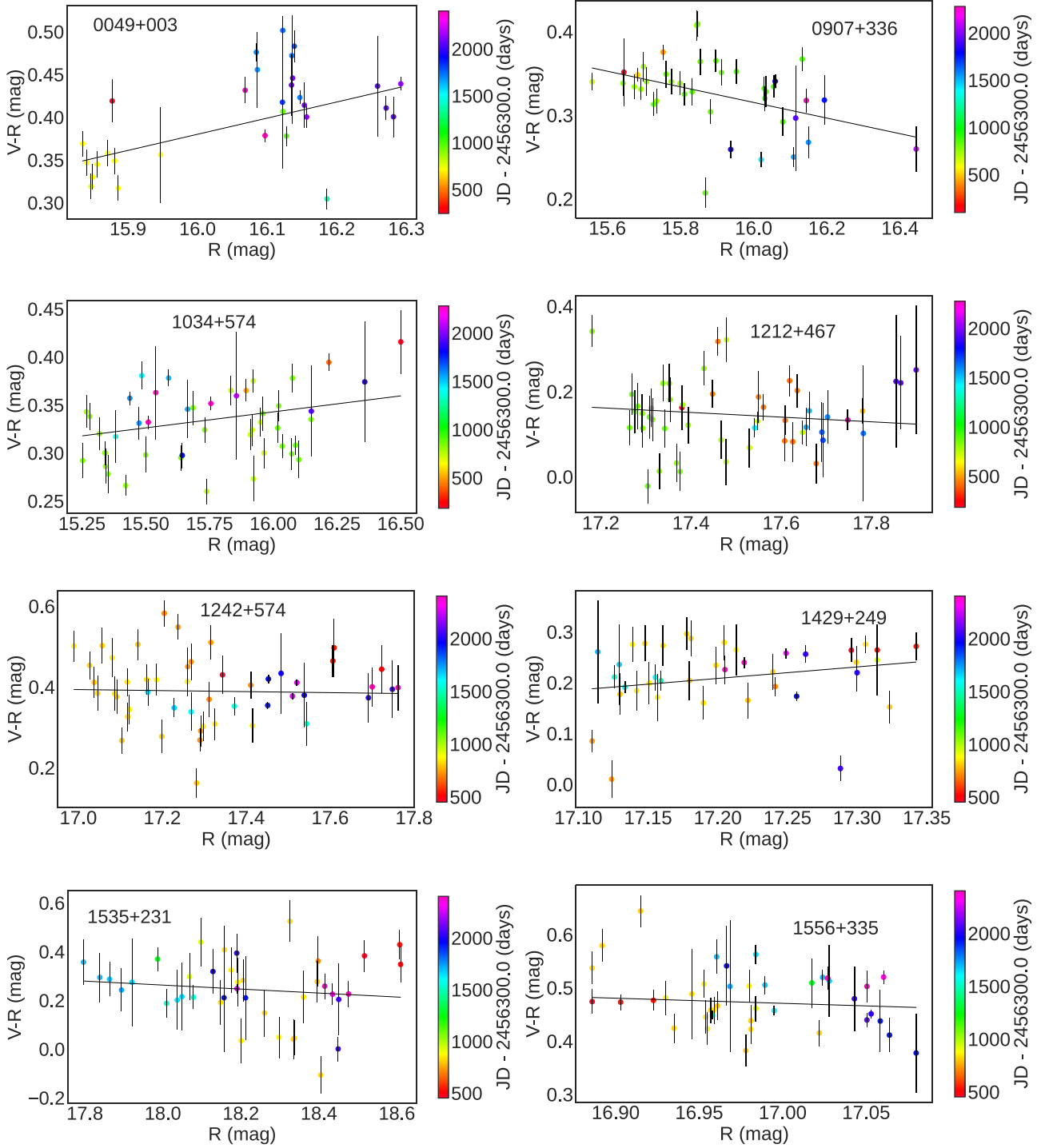
Figure C1. The correlation between colour indices $V - R$ and R-band magnitude of 0049+003, 0907+336, 1034+574, 1212+467, 1242+574, 1429+249, 1535+231, 1556+335, 1607+604, 1612+378, 1722+119, and 1741+597, with colour bars which indicate the progression of time. Details for all sources can be found in Table 6.
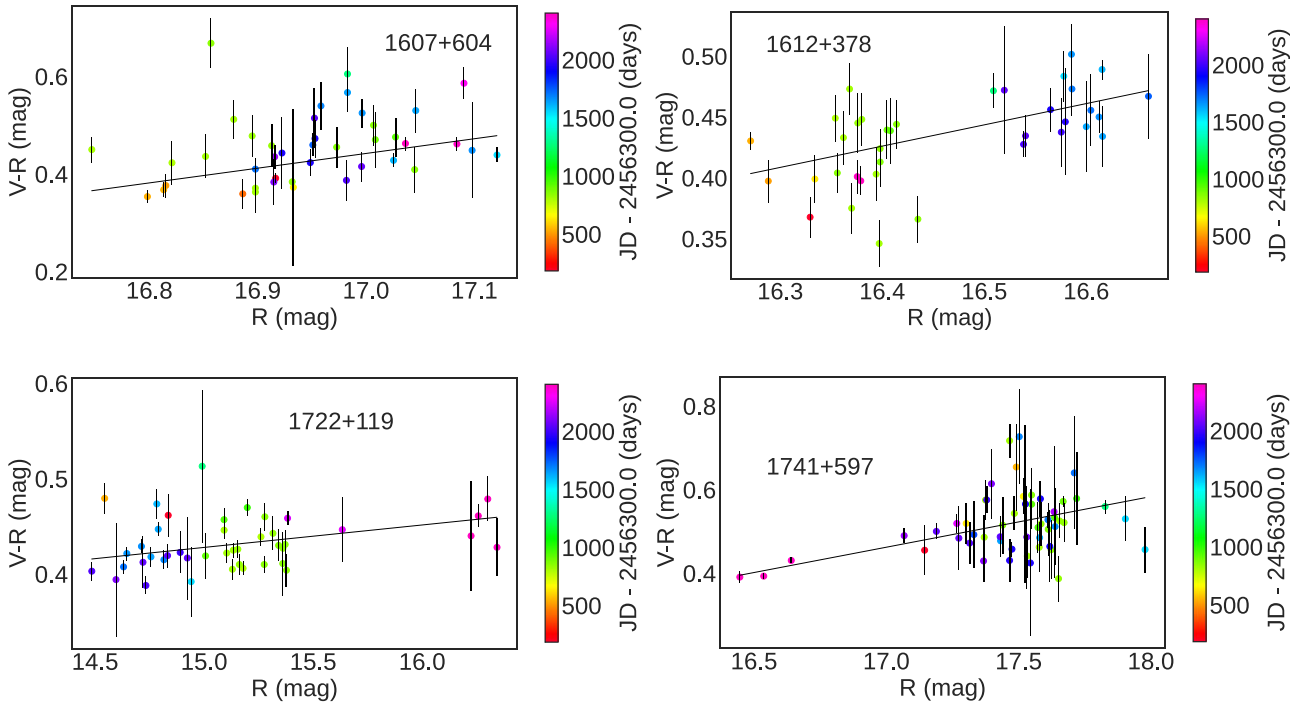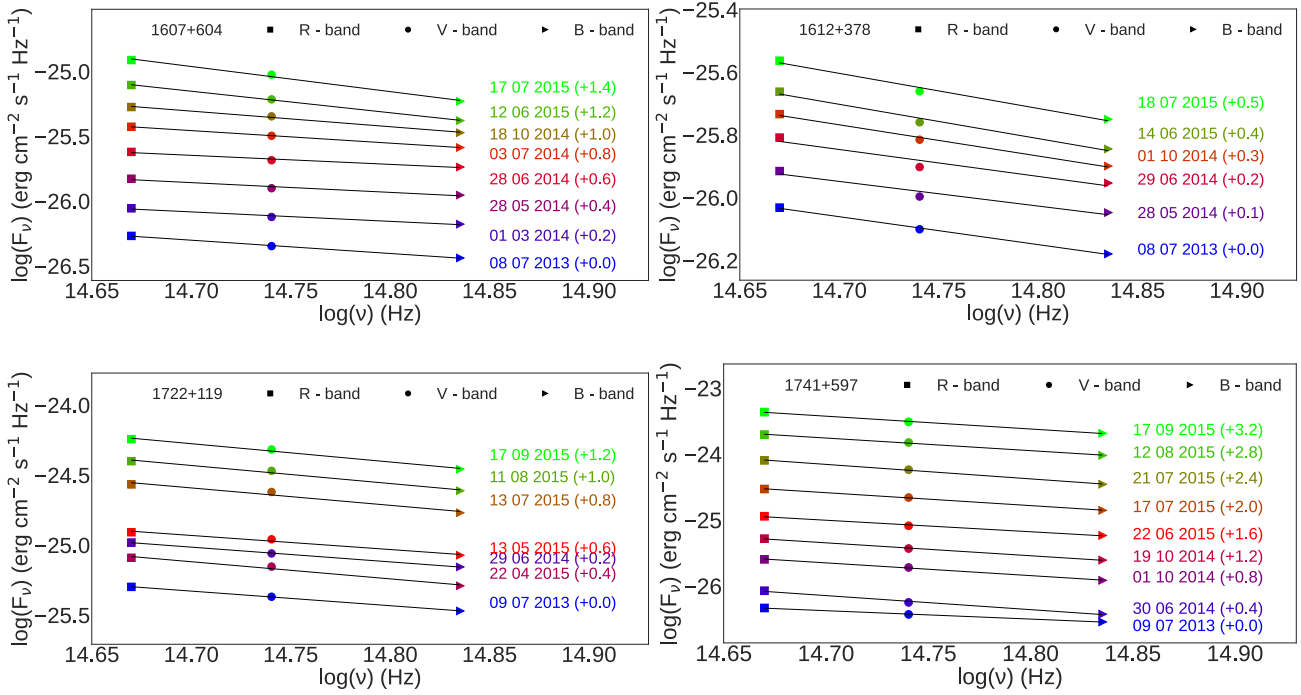
Figure C1. *continued.*

APPENDIX D: SED
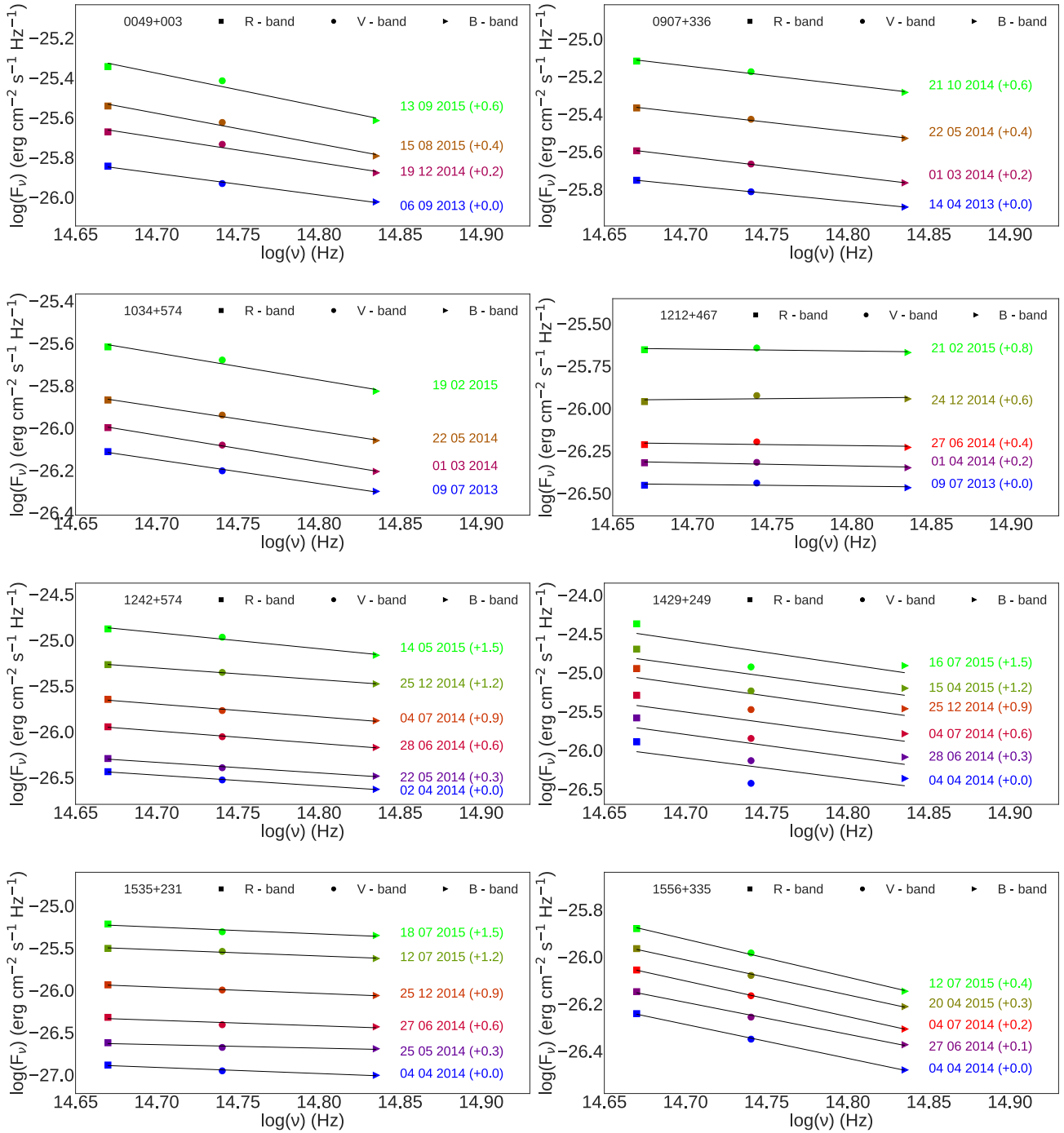
Figure D1. SED of the sources.

Figure D1. *continued.*

APPENDIX E: VARIATIONS OF OPTICAL SPECTRAL INDEX DURING TIME
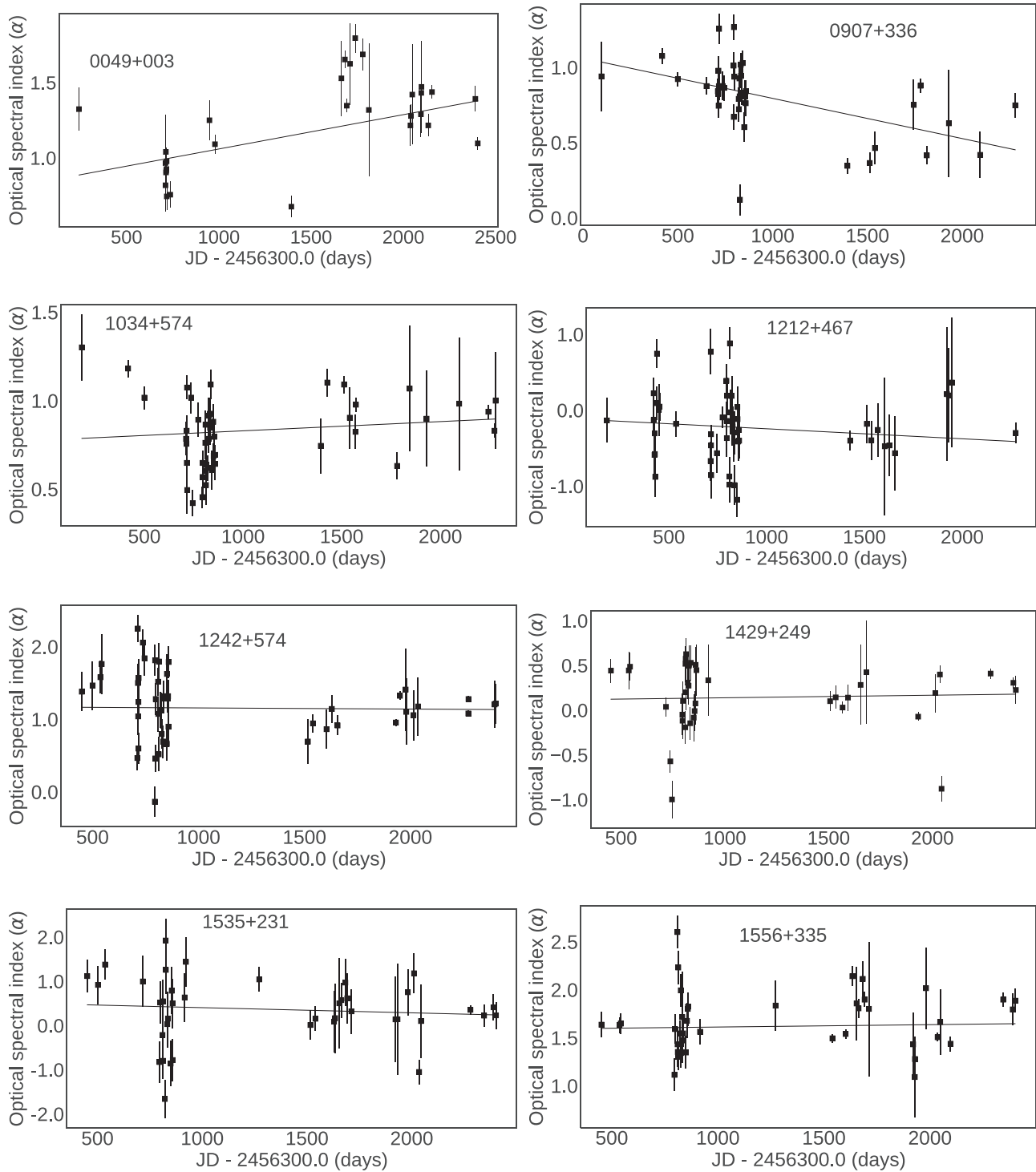
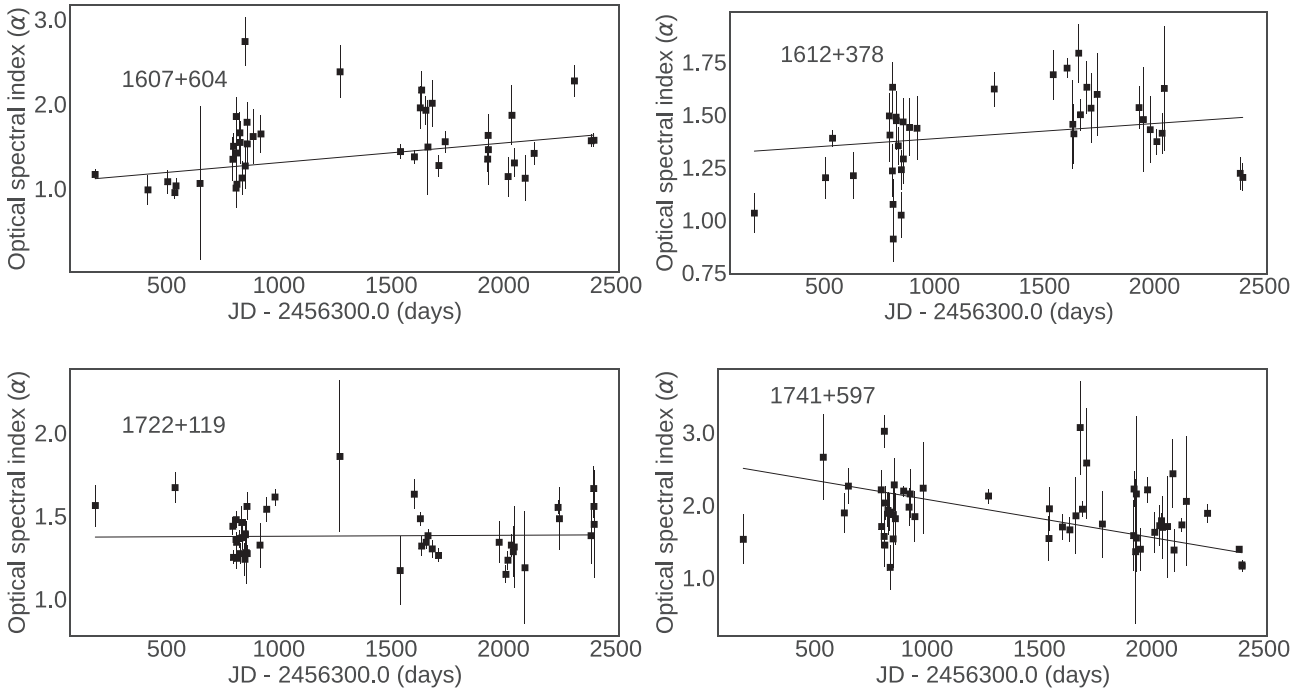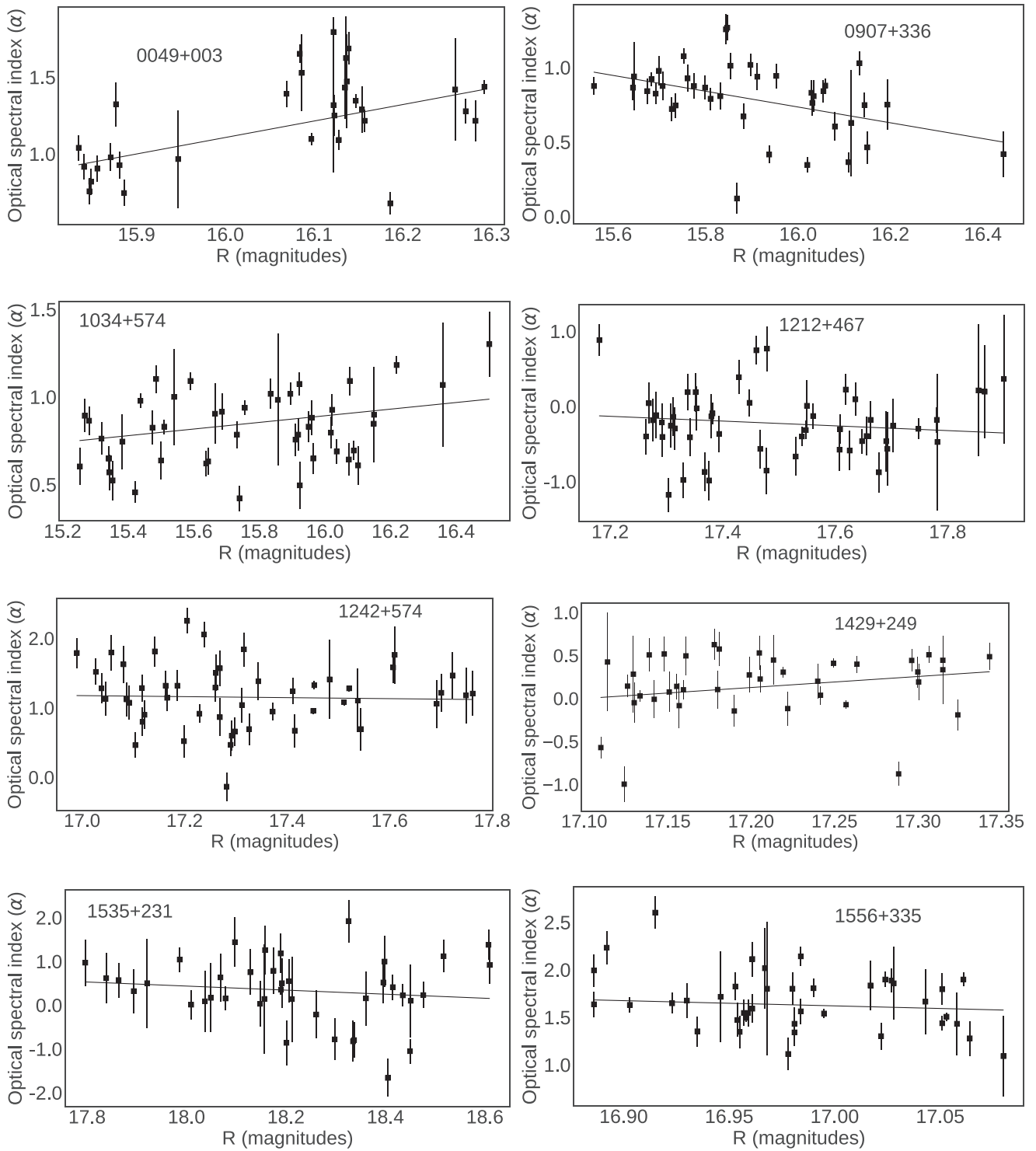**Figure E1.** Spectral index versus time.

Figure E1. *continued.*

APPENDIX F: VARIATIONS OF OPTICAL SPECTRAL INDEX WITH RESPECT TO *R* MAGNITUDE

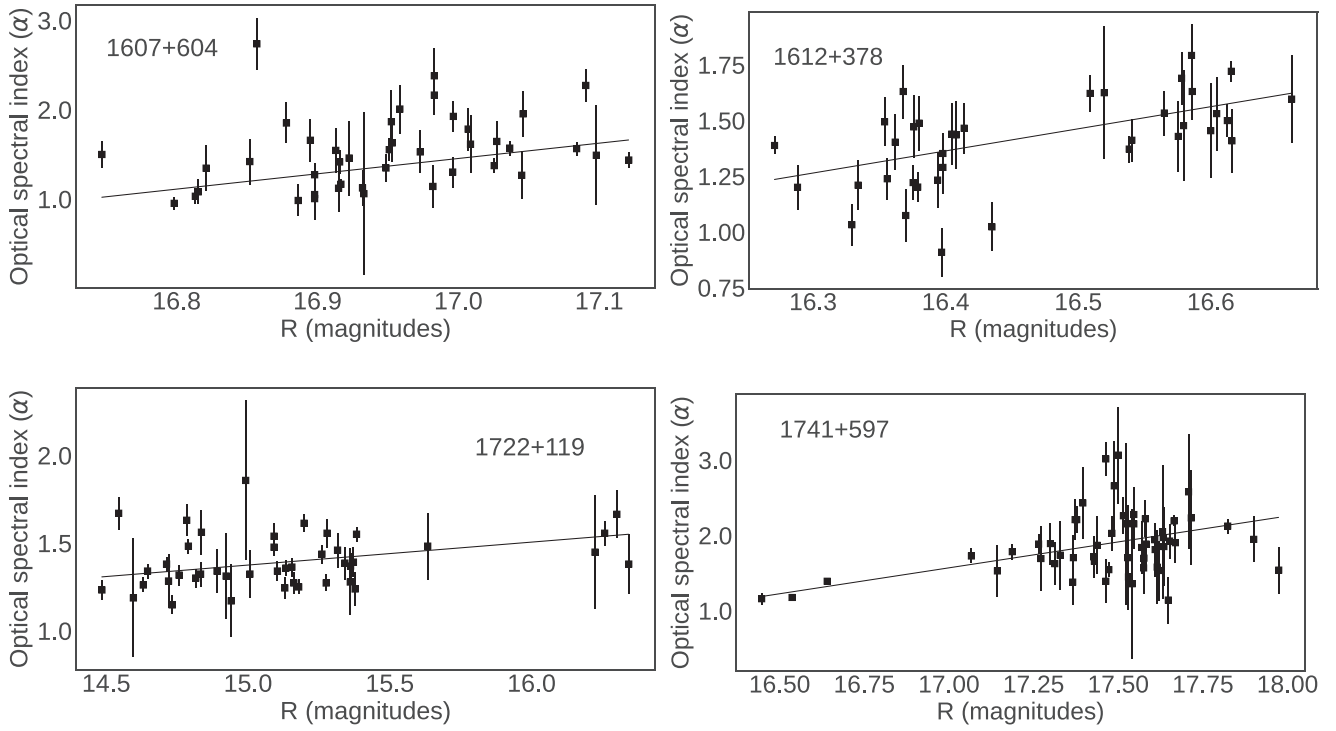**Figure F1.** Spectral index versus *R* mag.

Figure F1. *continued.*

This paper has been typeset from a TEX/LATEX file prepared by the author.